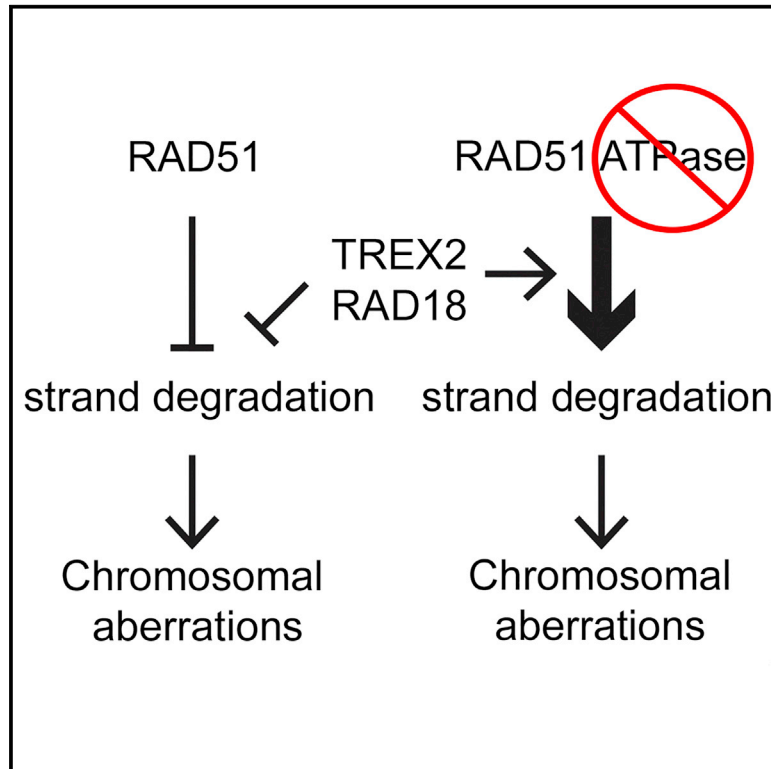


TREX2 Exonuclease Causes Spontaneous Mutations and Stress-Induced Replication Fork Defects in Cells Expressing RAD51^{K133A}

Graphical Abstract



Authors

Jun Ho Ko, Mi Young Son, Qing Zhou, ..., Cristina Montagna, Lumir Krejci, Paul Hasty

Correspondence

hastye@uthscsa.edu

In Brief

Ko et al. find that TREX2's exonuclease activity causes mutations, RF stalls, and strand degradation in cells expressing RAD51^{K133A}. RAD18 deletion and PCNA overexpression reduce mutations, implicating DNA damage tolerance. Deleting TREX2 in PARP1-deficient or FANCB mutant cells increases strand degradation that is rescued by TREX2^{H188A}, showing that TREX2's catalytic activity is unimportant.

Highlights

- In RAD51^{K133A} cells, TREX2's exonuclease causes mutations and stalled forks
- RAD18 and PCNA ubiquitination influence mutation levels in RAD51^{K133A} cells
- TREX2^{H188A} rescues strand degradation in cells defective for PARP1 or FANCB
- TREX2^{H188A} binds to UBC13 and rescues PCNA ubiquitination



Article

TREX2 Exonuclease Causes Spontaneous Mutations and Stress-Induced Replication Fork Defects in Cells Expressing RAD51^{K133A}

Jun Ho Ko,^{1,8,9} Mi Young Son,^{1,3,9} Qing Zhou,^{1,9} Lucia Molnarova,⁶ Lambert Song,⁴ Jarmila Mlcouskova,⁷ Atis Jekabsons,^{5,7} Cristina Montagna,⁴ Lumir Krejci,^{5,6,7} and Paul Hasty^{1,2,3,10,*}

¹Department of Molecular Medicine and Institute of Biotechnology, University of Texas Health San Antonio, San Antonio, TX 78245, USA

²The Cancer Therapy & Research Center, University of Texas Health San Antonio, San Antonio, TX 78229, USA

³Sam and Ann Barshop Institute for Longevity and Aging Studies, University of Texas Health San Antonio, San Antonio, TX 78245, USA

⁴Department of Genetics, Albert Einstein College of Medicine, Yeshiva University, Bronx, NY 10461, USA

⁵National Centre for Biomolecular Research, Masaryk University, Kamenice 5/A7, 625 00 Brno, Czech Republic

⁶Department of Biology, Masaryk University, Kamenice 5/A7, 625 00 Brno, Czech Republic

⁷International Clinical Research Center, Center for Biomolecular and Cellular Engineering, St. Anne's University Hospital Brno, Pekarska 53, 656 91 Brno, Czech Republic

⁸Present address: Potency Assay Group, Novartis Gene Therapies, San Diego, CA 92121, USA

⁹These authors contributed equally

¹⁰Lead Contact

*Correspondence: hastye@uthscsa.edu

<https://doi.org/10.1016/j.celrep.2020.108543>

SUMMARY

DNA damage tolerance (DDT) and homologous recombination (HR) stabilize replication forks (RFs). RAD18/UBC13/three prime repair exonuclease 2 (TREX2)-mediated proliferating cell nuclear antigen (PCNA) ubiquitination is central to DDT, an error-prone lesion bypass pathway. RAD51 is the recombinase for HR. The RAD51 K133A mutation increased spontaneous mutations and stress-induced RF stalls and nascent strand degradation. Here, we report in RAD51^{K133A} cells that this phenotype is reduced by expressing a TREX2 H188A mutation that deletes its exonuclease activity. In RAD51^{K133A} cells, knocking out RAD18 or overexpressing PCNA reduces spontaneous mutations, while expressing ubiquitination-incompetent PCNA^{K164R} increases mutations, indicating DDT as causal. Deleting TREX2 in cells deficient for the RF maintenance proteins poly(ADP-ribose) polymerase 1 (PARP1) or FANCB increased nascent strand degradation that was rescued by TREX2^{H188A}, implying that TREX2 prohibits degradation independent of catalytic activity. A possible explanation for this occurrence is that TREX2^{H188A} associates with UBC13 and ubiquitinates PCNA, suggesting a dual role for TREX2 in RF maintenance.

INTRODUCTION

DNA damage tolerance (DDT) is an error-prone pathway that bypasses lesions to stabilize replication forks (RFs) and enable their progression. DDT contributes to the stability of RFs when they encounter DNA lesions and blocking structures through translesion synthesis (TLS), RF reversal, template switching (TS), and repriming (Pilzecker et al., 2019). TLS and TS are two branches of DDT (Branzei and Psakhye, 2016; Pilzecker et al., 2019), and both are controlled by posttranslational modifications of proliferating cell nuclear antigen (PCNA). To mediate TLS, a replisome might skip a lesion, leaving an unreplicated gap for PrimPol primase to reinitiate DNA synthesis (McCulloch and Kunkel, 2008). RAD6/RAD18 monoubiquitinate PCNA K164 to induce TLS by switching polymerase (pol) δ/ϵ with a TLS polymerase (Prakash et al., 2005). Many of the TLS polymerases are mutagenic due to their low stringency (McCulloch and Kunkel, 2008). Ubiqui-

tin-conjugating enzyme variant UBC13/MMS2 polyubiquitinate PCNA K164 to induce TS with the assistance of HLTF (helicase-like transcription factor) or SHPRH in mammals (Krijger et al., 2011; Motegi et al., 2008). TS occurs between two nascent strands within a RF. This can involve the formation of cruciform intermediates between paired sister chromatids (Branzei and Foiani, 2007). Failure to properly resolve these structures provokes unscheduled recombination between nonallelic repeats, resulting in genomic instability (Hu et al., 2013). Thus, both TLS and TS can be mutagenic.

Three prime repair exonuclease 2 (TREX2) is hypothesized to influence DDT (Hu et al., 2013). TREX2 was found to physically associate with UBC13 using both *in vitro* and *in vivo* methodologies, and their association increased with exposure to UV light. In addition, TREX2 knockout cells exhibited a reduction of PCNA ubiquitination compared with wild-type (WT) cells. Furthermore, cells deleted for RAD18 and TREX2 showed a similar phenotype



including decreased levels of inverted mismatch repeat fusion, poor ability to ubiquitinate PCNA, and increased levels of stalled RFs (Hu et al., 2013). Therefore, TREX2 function is likely associated with DDT and suggests that TREX2 could be mutagenic.

TREX2 is most closely related to TREX1, and both are non-processive 3'–5' exonucleases that remove 3' mismatches from DNA (Chen et al., 2007; Mazur and Perrino, 1999, 2001; Perrino et al., 2005). TREX1 is a component of the SET complex that degrades 3' ends of nicked DNA during granzyme-A-mediated cell death, and mutations in TREX1 result in a variety of autoimmune diseases (Tao et al., 2019); yet, the biological function of TREX2 is not well understood. TREX2 knockout cells or cells expressing a catalytic mutant that ablates exonuclease activity (H188A) (Chen et al., 2007) have a minor phenotype (Dumitrache et al., 2009, 2011). They exhibited decreased levels of spontaneous sister chromatid exchanges and increased levels of spontaneous broken chromatids. These alterations were not due to defective double-strand break (DSB) repair because exposing TREX2^{null} cells to DNA damaging agents failed to increase breaks. Furthermore, TREX2^{null} cells exhibited increased levels of DSB repair (Dumitrache et al., 2011), and TREX2^{null} cells or expression of the H188A mutant exhibited a decrease in fusing inverted mismatched repeats (Hu et al., 2013), indicating a potential role in DDT.

Homologous recombination (HR) is a tumor suppressor pathway (Roy et al., 2011) that repairs DNA DSBs and maintains stalled RFs (Carr and Lambert, 2013; Petermann et al., 2010; Son and Hasty, 2019). For DSB repair, the RAD51 recombinase forms a filament on single-stranded DNA (ssDNA) that searches and invades a homologous substrate provided by the sister chromatid. It also forms a filament at gaps associated with RFs not coupled with DSBs (Sirbu et al., 2011). RAD51 protects stalled RFs from MRE11-mediated nucleolytic degradation and promotes fork reversal and restart, thereby maintaining continuous DNA synthesis (Hashimoto et al., 2010; Kondratova et al., 2015; Mijic et al., 2017; Schlacher et al., 2011). The Walker A motif in RAD51 contains a conserved K that binds and hydrolyses ATP. The K133A mutant ablated ATP binding and exhibited dramatic structural changes within the RAD51 filament and showed different kinetics of formation and disassembly of the filament that abolished the homology search and strand invasion (Chi et al., 2006; Špirek et al., 2018). Previously, we knocked in human RAD51 WT and K133A to the *Rad51* promoter in mouse embryonic stem (ES) cells. Compared with RAD51^{WT}, expression of RAD51^{K133A} caused an increase in RF stalls, hypersensitivity to a type I topoisomerase inhibitor (camptothecin [CPT]), enhanced ATR/CHK1 (ataxia telangiectasia and Rad3-related protein/checkpoint kinase 1) response, and elevated levels of gross chromosomal rearrangements (GCRs) (Kim et al., 2012). We then expressed human *RAD51* cDNA conjugated to EGFP and found that compared with RAD51^{WT}, the RAD51^{K133A} level was similar in the chromatin fraction but less RAD51^{K133A} was found at stressed RFs and DNA damage sites (Kim et al., 2012). Yet, the nature of the mechanistic origin for this phenotype, including the presence of GCRs, is not known.

Similar to DDT and HR, poly(ADP-ribose) polymerase 1 (PARP1) and the Fanconi anemia (FA) maintain RFs. PARP1 is a part of the DNA damage response network (Ghosal and

Chen, 2013), and its activity inhibits RECQ1 helicase to stabilize reversed RFs (RRFs). Exposing cells to olaparib (OLA; PARP1 inhibitor) reduced the level of RRFs (Berti et al., 2013; Sogo et al., 2002). FA repairs DNA interstrand crosslinks and protects stressed RFs (Kolinjivadi et al., 2020). The FA proteins BRCA2 (Breast Cancer 2) (Chen et al., 1998; Sharan et al., 1997), Fanconi anemia complementation group D2 (FANCD2) (Taniguchi et al., 2002), and RAD51C (Vaz et al., 2010) associate with RAD51. Furthermore, BRCA2 stabilized the RAD51 filament in FA-defective cells to protect RFs from degradation (Schlacher et al., 2011, 2012). Genetic mutations in the FA pathway caused chromosomal instability, developmental defects, bone marrow failure, and cancer (Wang, 2007). Previously we deleted exon 2 in mouse ESCs (embryonic stem cells) (*fancB*^{Δex2}) (Kim et al., 2011). FANCB is an essential member of the FA core complex (Meetei et al., 2004) that monoubiquitinates FANCD2 (Rajendra et al., 2014), and disrupting FANCB ablates core complex function (Huang et al., 2014). *FancB*^{Δex2} cells exhibited reduced cellular proliferation, hypersensitivity to the crosslinking agent mitomycin C (MMC), increased spontaneous and MMC-induced chromosomal abnormalities, reduced MMC-induced RAD51 foci, and absent MMC-induced FANCD2 foci.

Here, we aimed to understand the mechanism responsible for genome instability in RF maintenancedeficient cells. RAD51^{K133A}-expressing cells exhibited increased levels of spontaneous GCRs and increased levels of stress-induced stalled RFs and nascent strand degradation. However, TREX2 deletion or expression of the exonuclease mutant (H188A) reduced these events, indicating a role of TREX2's exonuclease activity in processing stalled RFs. RAD18 deletion and overexpression of PCNA^{WT} also reduced mutations in RAD51^{K133A}-expressing cells, while overexpression of ubiquitination-incompetent PCNA^{K164R} increased it. Deleting TREX2 in cells deficient for PARP1 or mutant for FANCB increased nascent strand degradation that was rescued by TREX2^{H188A}, implying that TREX2 protected against degradation independent of exonuclease activity. TREX2^{H188A} associated with UBC13 and rescued PCNA ubiquitination, suggesting a dual role for TREX2.

RESULTS

TREX2 Caused Spontaneous Mutations in RAD51^{K133A} Cells

We used genetically altered male mouse ESCs that were generated by targeting both *Rad51* and *Trex2* followed by introducing human WT or mutated *RAD51* and *TREX2* cDNAs back into their respective genes with Cre and Flip recombinases (Figure 1, see legend for a detailed description). Key to this sequential protocol is a floxed *miniHPRT* (hypoxanthine phosphoribosyl-transferase) that offers a dual-selection advantage of HAT (hypoxanthine, aminopterin, thymidine) and TG (6-thioguanine) for presence or absence of expression, respectively (Holcomb et al., 2007). The final product is cells that express one human RAD51 cDNA (WT or K133A) and one WT mouse RAD51 along with one human TREX2 cDNA (TREX2 is located to the X chromosome).

To characterize the biological impact of HR deficiency, two-color fluorescence *in situ* hybridization (FISH) on metaphase

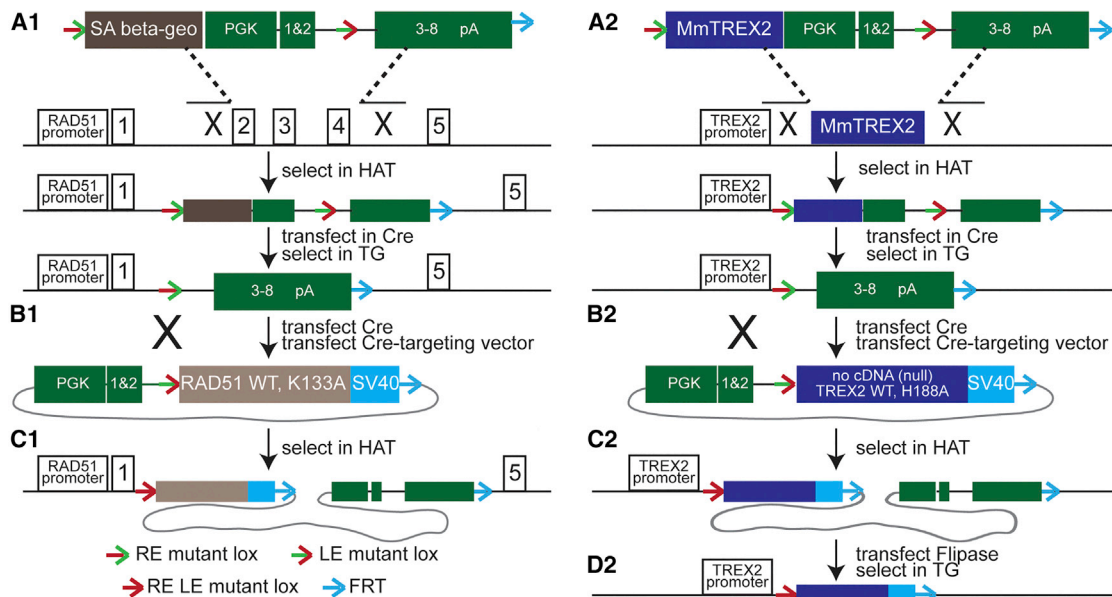


Figure 1. Knockout-Knockin into *Rad51* and *Trex2*

(A1) Schematics of replacement of *Rad51* exons 2–4 with *SAβgeo-miniHPRT* (Holcomb et al., 2007; Kim et al., 2012). *SAβgeo* is a fusion of β -galactosidase and neomycin phosphotransferase with a splice acceptor (SA) instead of a promoter so that cells will survive G418 selection only if a promoter/splice donor is trapped (Friedrich and Soriano, 1991). *MiniHPRT* contains a phosphoglycerate kinase (PGK) promoter with an intron that separates exons 1 and 2 from exons 3–8 and polyadenylation sequences. An *RE mutant loxP* (red green arrow) (Araki et al., 1997) flanks the 5' end, and a second *RE mutant loxP* was located in the intron of *miniHPRT*. An FRT (flippase recognition target, blue arrow) flanks the 3' end. Selection was done in G418+hypoxanthine, aminopterin, thymidine (HAT), and screening for targeted clones was done by PCR.

(A2) Schematics of *Trex2* knockout (Dumitriche et al., 2009). *Trex2* cDNA was replaced with mouse *Trex2* cDNA plus *miniHPRT*. Colonies were selected in HAT and screened for targeted clones by PCR.

(B1) The generation of *RAD51*^{+/3mH} cells. The 5' half of *miniHPRT* was removed by transfection with Cre recombinase followed by selection in TG and screened for removal of 5' *miniHPRT* by PCR.

(B2) The generation of *TREX2*^{+/3mH} cells. The 5' half of *miniHPRT* was removed by transfection with Cre recombinase followed by selection in TG and screened for removal of 5' *miniHPRT* by PCR.

(C1) Knockin of Cre mediated targeting vector with *RAD51* cDNA. Colonies were selected in HAT and screened for knockin by PCR.

(C2) Knockin of Cre mediated targeting vector with *TREX2* cDNA (empty vector [EV] is used for null). Colonies were selected in HAT, and screen for knockin was done by PCR.

(D2) Removal of plasmid backbone and *miniHPRT*. Cells were transfected with Flippase, and colonies were selected in TG and screened by PCR. The following sequential order was used to generate these cells: A1, B1, A2, B2, C2, D2, and C1.

spreads (MPSs) was used to screen for spontaneous GCRs in *RAD51* (WT, K133A) and *TREX2* (WT, null, H188A) cells. MPSs were stained with a telomeric probe (green), a major satellite repeat probe (red) in the pericentromere and counterstained with DAPI (blue) (Guenatri et al., 2004). A variety of chromosomal defects including fragments, segmental duplications, and Robertsonian translocations (RbTs) were observed (Figure 2A, left). The level of spontaneous aberrations was small in *RAD51*^{WT}-expressing cells independent of *TREX2* genotype (Figure 2A, compare lanes 1–3); yet, compared with *TREX2*^{WT}/*RAD51*^{WT}, cells expressing *TREX2*^{WT}/*RAD51*^{K133A} exhibited a 23-fold increase in spontaneous aberrations: 1.92 versus 0.083 abnormalities/MPS (Figure 2A, compare lanes 1 versus 4). By contrast, cells expressing *RAD51*^{K133A} along with either *TREX2*^{null} or *TREX2*^{H188A} exhibited only 0.19 to 0.028 abnormalities per MPS (Figure 2A, compare lanes 4 versus 5 and 6). Fragments, segmental duplications, and RbTs were all reduced (Figure S1), suggesting that *TREX2* nuclease activity is required for most of the spontaneous GCRs observed in HR-defective cells.

To further assess *TREX2*'s effect on genome stability, we tested *miniHPRT* loss of function (LOF) by survival in TG using cells containing one copy of *miniHPRT* located to chromosome 2 at the *Rad51* locus. Cells exhibited very few TG-resistant colonies when expressing *RAD51*^{WT} with *TREX2*^{WT}, *TREX2*^{null}, or *TREX2*^{H188A} (Figure 2B, lanes 1–3). However, compared with *TREX2*^{WT}/*RAD51*^{WT} cells, expression of *RAD51*^{K133A} in *TREX2*^{WT} cells showed a 46-fold increase in TG-resistant colonies (1.53% versus 0.033%) (Figure 2B, compare lanes 1 to 4). Furthermore, *RAD51*^{K133A} cells expressing *TREX2*^{null} or *TREX2*^{H188A} exhibited only 0.0094% or 0% TG-resistant colonies, respectively (Figure 2B, compare lanes 4 to 5 and 6), indicating a role of *TREX2* nuclease activity in LOF. To further investigate chromosomal aberrations, chromosome painting on MPSs was used to assess chromosome structural variants for *miniHPRT* LOF with a chromosome 2 probe (location of *Rad51*) and a locus-specific probe (LSP) that is positioned close to the long arm telomere. The parental *TREX2*^{WT}/*RAD51*^{WT} MPSs were analyzed, and they exhibited an inversion within chromosome 2 (Inv(2)) (Figure 2C);

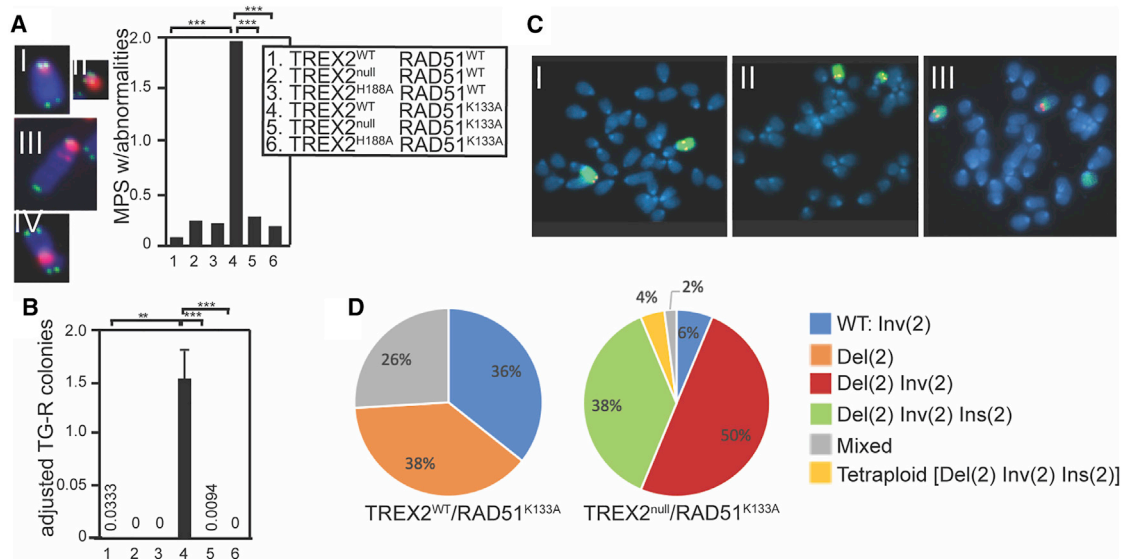


Figure 2. TREX2 Alteration Reduces Genomic Instability in RAD51^{K133A} Cells

(A and B) Refer to legend for numerical identification of genotypes in (A) and (B). (A) Left: representative examples of chromosomes: (I) normal, (II) fragment, (III) segmental duplication (SD), and (IV) Robertsonian translocation (RbT). Right: TREX2- deletion or TREX2^{H188A} expression reduced chromosomal aberrations in RAD51^{K133A} cells. At least 60 metaphase spreads (MPSs) were analyzed and counted for each genotype. Statistics: a chi-square test with Yates' correction and Fisher's exact test were performed using Prism8 software (GraphPad). (B) Measurement of *miniHPRT* LOF as TG-resistant (TG-R) colonies in RAD51^{K133A} cells deleted for TREX2 or expressing TREX2^{H188A}. Statistics: one-way ANOVA with Tukey's multiple comparisons test was performed using Prism8 software. Mean \pm SD, n = 3.

(C) Representative examples of MPSs hybridized with a chromosome 2 (ch2) probe and a locus-specific probe (LSP): (I) an inversion in ch2 (Inv(2)), (II) a deletion and an inversion within ch2 (Del(2), Inv(2)), and (III) a deletion and an insertion within ch2+ch2 without an LSP (Del(2), Inv(2), Ins(2)).

(D) Pie charts describing the percentages of chromosomal defects for TREX2^{WT}/RAD51^{K133A} (left) and for TREX2^{null}/RAD51^{K133A} (right). Statistics are represented by *p < 0.05, **p < 0.005, and ***p < 0.0005.

therefore, Inv(2) is considered WT. Between four and six MPSs were analyzed for each clone derived from TREX2^{WT}/RAD51^{K133A} and TREX2^{null}/RAD51^{K133A} TG-resistant clones. Analysis of TREX2^{WT}/RAD51^{K133A} showed that 36% of clones had the same karyotype as the WT cells, 38% contained a deletion on chromosome 2 (Del(2)) (Figure 2CII), and 26% exhibited a mixed phenotype (Inv(2) and Del(2)) suggestive of chromosome 2 instability. By contrast, only 6% of clones in TREX2^{null}/RAD51^{K133A} cells showed the same karyotype as WT cells; 50% showed a deletion and an inversion on chromosome 2 (Del(2), Inv(2)); 38% showed not only Del(2), Inv(2) but also an insertion of chromosome 2 (Del(2), Inv(2), Ins(2)) (Figure 2CIII); 4% were a tetraploidization of the preceding karyotype; and 2% contained cells with mixed karyotype. Thus, most, but not all, of the TREX2^{WT}/RAD51^{K133A} clones analyzed showed an obvious structural variation compared with the parental TREX2^{WT}/RAD51^{WT} MPSs (Figure 2D).

TREX2 Caused RF Defects in RAD51^{K133A} Cells

Previously, we showed that RAD51^{K133A} expression stalled RFs (Kim et al., 2012). To evaluate RF stalling and recovery, fiber analysis was performed on cells exposed to hydroxyurea (HU), a ribonucleotide reductase inhibitor (Meuth, 1989). Fibers were analyzed after exposing cells to 5-iodo-2'-deoxyuridine (IdU) for 20 min, followed by treatment with 0.5 mM HU for 1.5 h and then 5-chloro-2'-deoxyuridine (CldU) for 20 min. The percentage of unexposed cells undergoing RF stalling did not vary

for any of the genotypes (Figure 3A). However, after exposure to HU, there was increased stalled forks for all genotypes (Figure 3A). Only TREX2^{WT}/RAD51^{K133A} cells exhibited elevated levels of stalled RFs compared with TREX2^{WT}/RAD51^{WT} cells (Figure 3A). Deletion of TREX2 or expression of TREX2^{H188A} suppressed the increase in RF stalling in cells expressing RAD51^{K133A} (Figure 3A). In fact, comparing cells that expressed TREX2^{WT}/RAD51^{WT} to TREX2^{null}/RAD51^{K133A} or TREX2^{H188A}/RAD51^{K133A} showed no significant difference in the number of stalled RFs. Therefore, TREX2's exonuclease activity was required to stall RFs in cells expressing RAD51^{K133A}. These data indicate a role for TREX2's exonuclease activity in processing stalled RFs in cells expressing RAD51^{K133A}.

RAD51 protects stalled RFs (Bhat and Cortez, 2018; Rickman and Smogorzewska, 2019). Since MRE11 and DNA2 degrade the nascent strand, we analyzed the length of newly synthesized tracks in the presence of mirin, a MRE11 inhibitor (Schlacher et al., 2011) and C5, a DNA2 inhibitor (Liu et al., 2016). These agents are not highly specific, and their selectivity is not well established, so one must consider these factors when interpreting these data. For this experiment, the cells were labeled with 25 μ M IdU at 37°C for 30 min followed by treatment with 250 μ M CldU at 37°C for 30 min and then washed with fresh media three times. The labeled cells were treated with 4 mM HU \pm 50 μ M mirin (20 μ M C5) at 37°C for 5 h and then analyzed. With no HU treatment, compared with TREX2^{WT}/RAD51^{WT} cells, there was enhanced degradation when TREX2^{null}, TREX2^{H188A},

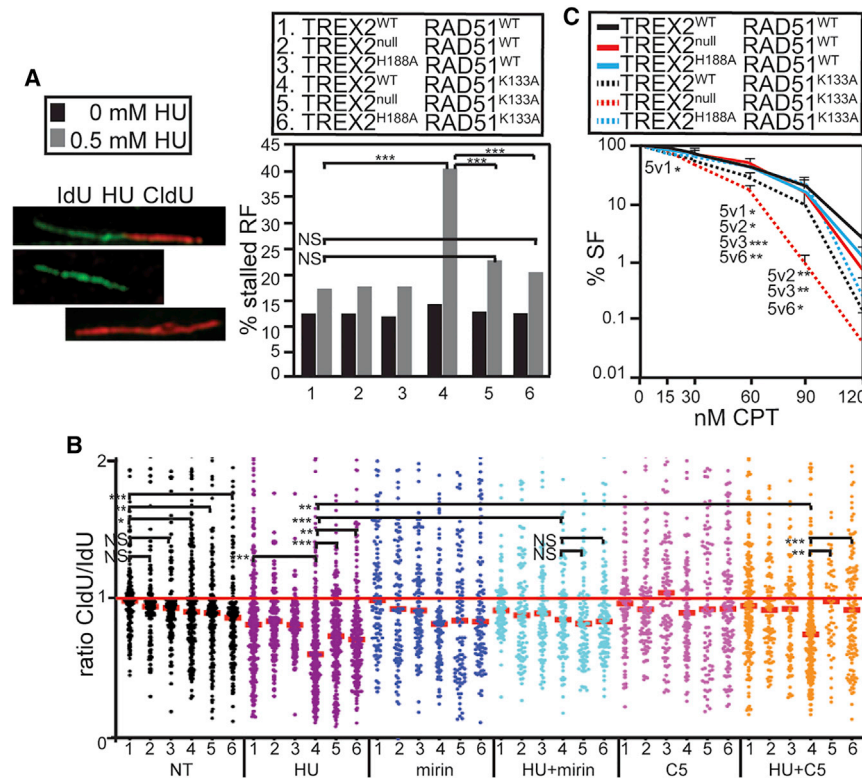


Figure 3. TREX2 Influences RFs in RAD51^{K133A} Cells

(A) Fiber analysis to analyze RF stalling. TREX2 stalls RFs in HsRAD51^{K133A} cells exposed to HU. Statistics: a chi-square test with Yates' correction and Fisher's exact test were performed using Prism8 software. At least 500 fibers were observed for each sample. For unexposed cells, all comparisons are $p > 0.25$.

(B) Fiber analysis of the impact of MRE11 and DNA2 on nascent strand degradation. Refer to legend for numerical identification of genotypes in (A). Red line: median for TREX2^{WT}/RAD51^{KA}. Statistics: Kruskal-Wallis test with Dunn's multiple comparison test analyzed by Prism8 software. At least 100 fibers were observed for each sample.

(C) Dose response to camptothecin (CPT) on indicated cell lines assessed by colony-forming assay. Compared with the other genotypes, TREX2^{null}/RAD51^{K133A} cells exhibited enhanced sensitivity after exposure to CPT. Statistics: two-way ANOVA with Dunnett's multiple comparisons test was performed using Prism8. Mean \pm SD, $n = 3$. Statistics are represented by * $p < 0.05$, ** $p < 0.005$, and *** $p < 0.0005$. NS, not significant.

or RAD51^{K133A} was expressed, demonstrating their protection of the nascent strand (Figure 3B). After exposure to HU, expression of RAD51^{K133A} resulted in massive degradation of the nascent strand compared with RAD51^{WT}. TREX2 deletion or expression of TREX2^{H188A} partially rescued this degradation (Figure 3B). Exposure to mirin reduced degradation of the nascent strand in TREX2^{WT}/RAD51^{K133A} cells, while expressing TREX2^{null} or TREX2^{H188A} had no further effect (Figure 3B). Similar to mirin, exposure to C5 reduced degradation of the nascent strand in TREX2^{WT}/RAD51^{K133A} cells; yet, unlike mirin, expression of TREX2^{null} or TREX2^{H188A} further reduced degradation of the nascent strand (Figure 3B). These data are consistent with TREX2's exonuclease activity contributing to stressed-induced RF stalling and nascent strand degradation.

RAD51 participates in RF reversal (Zellweger et al., 2015). Therefore, we tested cells for sensitivity to CPT using a colony forming assay. CPT is a type 1 topoisomerase inhibitor that causes RF reversal (Berti et al., 2013). Deletion of TREX2 enhanced the sensitivity of RAD51^{K133A} cells to CPT without altering it in RAD51^{WT} cells (Figure 3C). Furthermore, expression of TREX2^{H188A} did not enhance CPT sensitivity for RAD51^{K133A} cells. This is interesting since TREX2's exonuclease activity caused mutations, RF stalls, and nascent strand degradation, implicating that TREX2's exonuclease activity caused CPT hypersensitivity and that TREX2 had an exonuclease independent function.

We performed a nuclease protection assay to determine whether the observed nascent strand degradation of

RAD51^{K133A} correlates with its efficiency to protect ssDNA from TREX2 exonuclease activity. Electron micrographs showed RAD51^{WT} and RAD51^{K133A} formed filaments and rings on a short DNA substrate with a 35 bp overhang (Figure S2A). Increasing concentrations of purified RAD51^{WT} or RAD51^{K133A} were pre-assembled on a 5' fluorescently labeled DNA substrate, followed by the addition of 450 pM TREX2 exonuclease (Figure S2B). Whereas 1 μ M RAD51^{WT} was able to prevent 73% of DNA from degradation, 1 μ M RAD51^{K133A} protected only 38% of ssDNA from TREX2's exonuclease activity (Figures 4A and 4B). A nuclease protection assay was also performed with varying concentrations of RAD51^{WT} and RAD51^{K133A} to test whether a mixed saturated filament protected the nascent strand. We observed increased degradation of the DNA substrate corresponding to an increased concentration of RAD51^{K133A} (Figures 4C and 4D). These results are consistent with the enhanced level of nascent strand degradation observed in RAD51^{K133A}-expressing cells and suggest it is caused by increased nuclease accessibility of filaments with RAD51^{K133A}.

DDT Is Responsible for Spontaneous Mutations in RAD51^{K133A} Cells

We addressed whether DDT is responsible for the genomic instability observed in RAD51^{K133A} cells. Since TREX2 appears to influence DDT (Hu et al., 2013), we tested the effect of RAD18 on LOF of *miniHPRT*. RAD18 was mutated in cells using CRISPR-Cas9 technology (Figure 5A, left) and then RAD51^{K133A} was inserted adjacent to the *Rad51* promoter. RAD18 deletion reduced the level of spontaneous TG-resistant colonies in cells expressing RAD51^{K133A} from 0.75% to 0.008% (Figure 5A, right). In either *Rad18*^{+/+} or *rad18*^{-/-} cells, the tetracycline (tet)-on

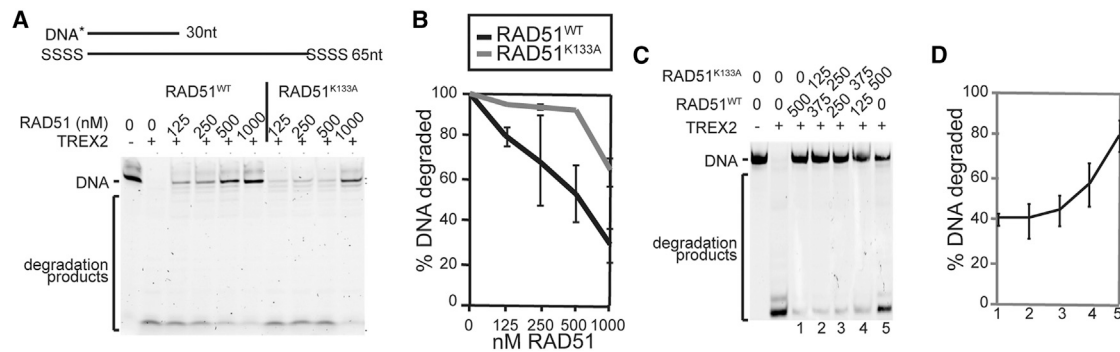


Figure 4. RAD51^{K133A} Has Lower Protection against TREX2's Exonuclease Activity Compared with RAD51^{WT}

(A) Nuclease protection assay. Top: a schematic representation of DNA substrate (30nt+65nt) containing phosphorothioate bonds (S) and labeled by fluorescein isothiocyanate (FITC) at 5' (asterisk). Bottom: representative gel of TREX2's nuclease activity on 5' FITC-labeled DNA substrate preassembled with increasing concentration of RAD51^{WT} or RAD51^{K133A}.

(B) Quantification of nuclease protection assay presented in (A). Mean \pm SD, n = 3.

(C) RAD51^{WT} partially suppresses the accessibility of RAD51^{K133A} filament to TREX2. Representative gel of TREX2's nuclease activity on 5' FITC-labeled DNA substrate with indicated mixture of RAD51^{WT} and RAD51^{K133A}.

(D) Quantification of nuclease protection assay presented in (C). Mean \pm SD, n = 3.

system was used by introducing the reverse tetracycline transactivator (rtTA) adjacent to the *Rad51* promoter and the tetracycline operator sequence – minimal cytomegalovirus (tetO-mCMV) promoter that expresses either RAD51^{WT} or RAD51^{K133A} in the opposite direction (Figure S3) (Choi et al., 2011). Adding doxycycline (dox) to the RAD18^{+/+}/RAD51^{K133A} cells increased the number of TG-resistant colonies by 18-fold (Figure 5B, compare lanes 1 to 2). This increase required both RAD51^{K133A} (Figure 5B, compare lanes 2 to 3) and RAD18 (Figure 5B, compare lanes 2 to 4). These data indicate that RAD18, similar to TREX2, was essential for generating the RAD51^{K133A}-induced TG-resistant colonies and imply that DDT is responsible for genome instability.

We tested the effect of PCNA K164 ubiquitination on generating spontaneous TG-resistant colonies in RAD51^{K133A} expressing cells since PCNA K164 ubiquitination is a critical marker for DDT (Hendel et al., 2011). Cells targeted at *Rad51* and *Top3 β* (Kim et al., 2008) were used with the 3' half of *miniHPRT*. Into these cells we inserted a 3XFLAG-human PCNA (WT or K164R) adjacent to the *Top3 β* promoter (Kim et al., 2008). We also inserted an empty vector (EV) into the same location. Next, flippase was used to delete *miniHPRT* and the backbone, and RAD51^{WT} or RAD51^{K133A} was targeted adjacent to the *Rad51* promoter. iPOND was used to verify the association of 3XFLAG-PCNA^{WT} and 3XFLAG-PCNA^{K164R} with nascent DNA at RFs. The expression levels of 3XFLAG-PCNA^{WT} and 3XFLAG-PCNA^{K164R} were comparable (Figure 5C). Little difference was observed in the recovery of TG-resistant colonies between cells expressing RAD51^{WT} along with the EV or 3XFLAG-PCNA^{WT} or 3XFLAG-PCNA^{K164R} (Figure 5D). By contrast, there were 8.57-7.6-fold fewer TG-resistant colonies recovered for RAD51^{K133A} cells expressing 3XFLAG-PCNA^{WT} compared with EV (Figure 5D, compare lanes 4 to 5). This observation implicates ubiquitinated PCNA is rate limiting. Furthermore, expression of 3XFLAG-PCNA^{K164R} increased the recovery of TG-resistant colonies by 1.54~0.7-fold compared with EV (Figure 5D, compare lanes 4 to 6). These data confirm that PCNA ubiquitination status

influences mutations in RAD51^{K133A} cells and provides more evidence that DDT is the causal mechanism for generating spontaneous mutations in RAD51^{K133A} cells.

TREX2 Protected against Nascent Strand Degradation in Cells with Defective PARP1 or FANCB

We wanted to determine whether the impact of deleting TREX2's exonuclease activity is limited to unstable RAD51 filaments, so we analyzed cells defective for either PARP1 or FANCB. PARP1-deficient cells were analyzed since PARP1 inhibits RECQ1 to stabilize RRFs (Berti et al., 2013; Sogo et al., 2002). FANCB mutant cells were analyzed since it is a part of the core complex that monoubiquitinates FANCD2 and since the FA pathway protects stressed RFs (Kolinjivadi et al., 2020).

Cells were exposed to a PARP1 inhibitor, OLA. OLA interferes with PARP1's inhibition of the RECQ1 helicase, ultimately destabilizing RRFs (Berti et al., 2013; Sogo et al., 2002). Compared with no treatment (NT), RAD51^{WT} cells that express TREX2 (WT, null, H188A) showed a trend of increased fiber degradation after exposure to HU (Figure 6A, compare NT lanes 1-3 to HU lanes 1-3). Yet for RAD51^{WT} cells expressing TREX2^{null}, there was significant degradation when OLA was added to HU (Figure 6A, compare HU lane 2 to HU+OLA lane 2), and this degradation was rescued with expression of either TREX2^{WT} or TREX2^{H188A} (Figure 6A, compare HU+OLA lane 2 to 1 and 3), implying that TREX2's exonuclease activity was responsible for the degradation and that TREX2 had an exonuclease-independent function. Cells were exposed to only OLA to determine the impact that HU-mediated replication stress had on PARP1-deficient TREX2 (WT, null, H188A)/RAD51^{WT} cells. For RAD51^{WT} cells expressing TREX2^{null}, there was significant degradation after exposure to OLA (Figure 6A, compare NT lane 2 to OLA lane 2), and expression of TREX2^{WT} or TREX2^{H188A} displayed a trend demonstrating rescue (Figure 6A, compare OLA lane 2 to OLA lanes 1 and 3) similar to the HU+OLA results, implying strand degradation could be seen without HU-mediated stress. Perhaps OLA-mediated PARP1 inhibition induced replication

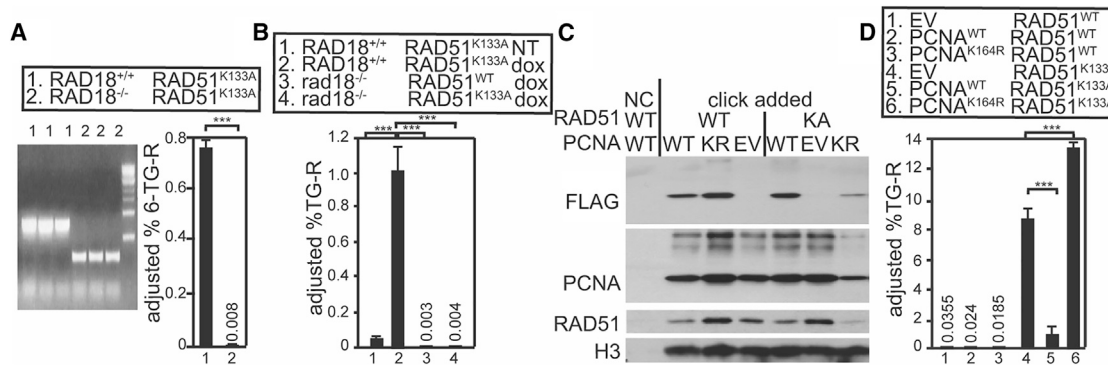


Figure 5. DDT Causes Genomic Instability in RAD51^{K133A} Cells

(A) RAD18 deleted cells reduced the level of mutations in RAD51^{K133A} cells. Left: detection of RAD18 knockout cells using PCR amplification; sample 1 is wild-type controls and sample 2 is *rad18*^{-/-} cells. The PCR fragment was sequenced, and exon 1 was deleted. Right: measurement of *miniHPRT* LOF in RAD51^{K133A} cells in RAD18^{+/+} or *rad18*^{-/-} cells. Statistics: a Student's t test was performed using Prism8 software. Mean ± SD, n = 3.

(B) RAD18 deleted cells reduce the level of mutations in RAD51^{K133A} cells using the tet-inducible system. Statistics was performed using one-way ANOVA with Sidák's multiple comparisons test by Prism8 software. Mean ± SD, n = 3.

(C) iPOND of 3XFLAG-PCNA^{WT} and 3XFLAG-PCNA^{K164R} in RAD51^{WT} and RAD51^{K133A} cells. EV: the vector without cDNA cloned into it. Individual proteins detected by corresponding antibodies are indicated. NC, no click chemistry used (click chemistry is to covalently tag EdU with biotin using the copper-catalyzed click reaction [Sirbu et al., 2012]).

(D) Quantification of effect of PCNA on *miniHPRT* LOF in RAD51^{K133A} cells. Expression of 3XFLAG-PCNA^{WT} decreased *miniHPRT* LOF by ~8.57-fold, while expression of 3XFLAG-PCNA^{K164R} increased loss of *miniHPRT* LOF by ~1.54-fold in RAD51^{K133A} cells compared with EV. Statistics was performed the same as in (B). Mean ± SD, n = 4

stress. A comparison between TREX2^{null}/RAD51^{WT} cells exposed to either OLA or OLA+HU showed that HU increased the level of degradation (Figure 6A, compare OLA lane 2 to HU+OLA lane 2), implying that HU and OLA caused strand degradation in an additive manner. Compared with cells with NT, HU significantly increased fiber degradation for RAD51^{K133A} cells (Figure 6A, compare NT lanes 4–6 to HU lanes 4–6), and OLA ameliorated this degradation independent of TREX2 (Figure 6A, compare HU lanes 4–6 to HU+OLA lanes 4–6), implying that PARP1 increased degradation with a faulty RAD51 filament without TREX2 involvement.

We tested the FA pathway in TREX2 (WT, null, H188A) cells that were deleted for *FancB* exon 2. *FancB*^{Δex2} cells (Kim et al., 2011) were targeted for TREX2 followed by insertion of TREX2 (WT, null, H188A) adjacent to the *Trex2* promoter (Figures 1A2–1C2). For NT, *FancB*^{Δex2} cells exhibited enhanced nascent strand degradation and deleting TREX2 modestly enhanced fiber degradation (Figure 6B, compare NT lanes 3 to 5), and expression of either TREX2^{WT} (p = 0.2276) or TREX2^{H188A} (p = 0.0897) showed a trend of less degradation. This further implies that TREX2's exonuclease activity was responsible for the degradation and that TREX2 had an exonuclease-independent function. Compared with cells with NT, HU significantly increased fiber degradation for *fancB*^{Δex2} cells (Figure 6B, compare NT lanes 4 and 6 to HU lanes 4 and 6) independent of TREX2 (Figure 6B, HU lanes 4–6), implying that FA-mediated stabilization of HU-stressed RFs decreased degradation without TREX2 involvement.

TREX2 Ubiquitinates PCNA Independent of Its Exonuclease Activity

The results shown in Figures 6A and 6B suggest that TREX2 functions independent of its exonuclease activity. We reported

that TREX2 associated with UBC13, but not with MMS2 (Hu et al., 2013). Therefore, we tested the ability of TREX2^{H188A} to associate with UBC13 and with MMS2. Like TREX2^{WT}, TREX2^{H188A} associated with UBC13, but not MMS2, by glutathione S-transferase (GST) pull-down (Figure 6C); thus, the H188A mutation did not interfere with this function. UBC13/MMS2 polyubiquitinates PCNA K164 in response to replication stress, and we previously showed that TREX2 is critical for ubiquitinating PCNA K164 (Hu et al., 2013). Therefore, we tested whether TREX2's exonuclease activity facilitated endogenous PCNA ubiquitination after UV light exposure. Deleting TREX2 in cells exposed to UV light reduced endogenous PCNA ubiquitination (Figure 6D, compare lanes 1 and 2), as we previously observed (Hu et al., 2013). Expression of TREX2^{WT} (Figure 6D, compare lanes 1 and 2 to 3) and TREX2^{H188A} (Figure 6D, compare lanes 1 and 2 to 4) rescued PCNA ubiquitination. These observations suggest that TREX2 contributes to RF maintenance at two points in the pathway: first PCNA ubiquitination and second exonuclease activity after PCNA ubiquitination.

DISCUSSION

RF maintenance is critical for preserving genome integrity. As a part of RF maintenance, BRCA2 and other recombination mediators assemble the RAD51 filament (Krejci et al., 2012; San Filippo et al., 2006; Sigurdsson et al., 2001) to suppresses nucleolytic degradation and promote fork reversal and restart (Hashimoto et al., 2010; Kondratova et al., 2015; Mijic et al., 2017; Schlacher et al., 2011). PARP1 inhibits RECQ1 helicase to stabilize RRFs (Berti et al., 2013; Sogo et al., 2002). FA proteins such as BRCA2 (Chen et al., 1998; Sharan et al., 1997) associate with RAD51 to protect RFs from degradation (Schlacher et al., 2011, 2012). DDT also contributes to RF

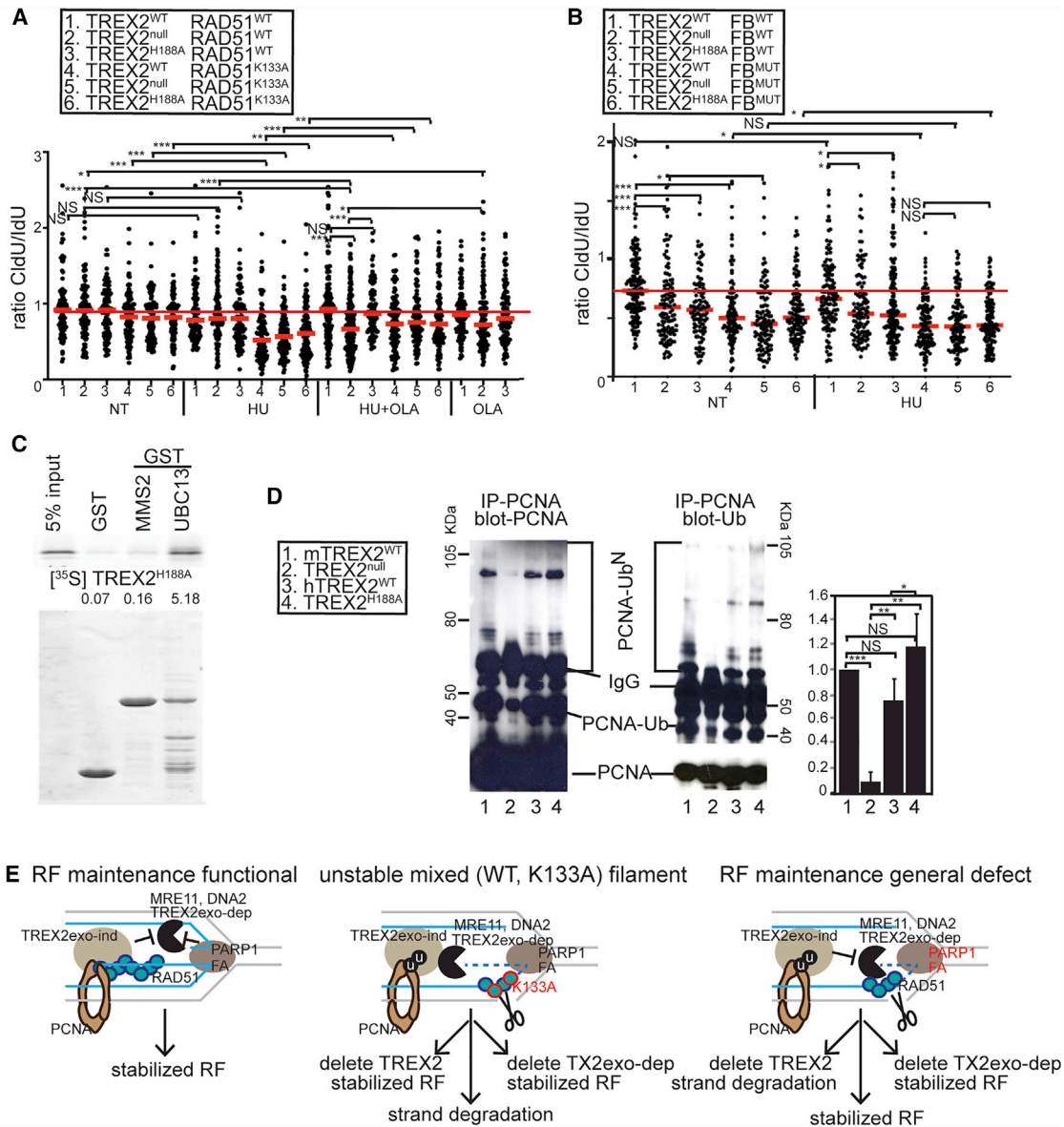


Figure 6. TREX2 Has a Dual Function during RF Maintenance

(A) Nascent strand degradation observed in TREX2 (WT, null, H188A)/RAD51 (WT, K133A) cells exposed to OLA. Kruskal-Wallis test with Dunn's multiple comparisons test was performed by Prism8 software. At least 100 fibers were observed for each sample.

(B) Nascent strand degradation observed in TREX2 (WT, null, H188A)/FANCB (WT, $\Delta ex2$) cells. Kruskal-Wallis test with Dunn's multiple comparisons test was performed by Prism8 software. At least 100 fibers were observed for each sample.

(C) GST pull-down of ³⁵S-labeled TREX2^{H188A} with UBC13.

(D) Analysis of PCNA ubiquitination on cells expressing TREX2^{H188A} (HA). Left: anti-PCNA immunoprecipitation (IP), anti-PCNA western blot. Middle: anti-PCNA IP, anti-ubiquitin (Ub) western blot. Right: quantification of PCNA-Ub^N, average of three experiments. Statistics are represented by NS, *p < 0.05, **p < 0.005, and ***p < 0.0005.

(E) Model of TREX2 causing nascent strand degradation in RF maintenance defective cells. Left (RF maintenance functional): fully functional RAD51^{WT} filament (blue circle with a dark blue circumference) prohibits excessive exonuclease activity (TREX2^{exo-dep}, black Pac-Man). DDT (light brown oval) with TREX2 (independent of its exonuclease function, TREX2^{exo-ind}). PARP1 and FA (dark brown oval) inhibits degradation and stabilizes the RF. Middle (unstable RAD51^{WT}+RAD51^{K133A} filament): HR is defective due to an unstable RAD51 filament caused by the K133A mutation (blue circle with a red circumference). DDT not only ubiquitinates PCNA to prevent RF collapse but also predisposes cells to mutations due to exonuclease activity from TREX2, MRE11, and DNA2. Right (RF maintenance general defect): PCNA polyubiquitination is essential to protect the nascent strand from degradation when PARP1 or FA (red script) is defective. A decrease in PCNA ubiquitination causes strand degradation (TREX2^{null}) that is corrected with expression of either TREX2^{WT} or TREX2^{H188A}.

stabilization (Pilzecker et al., 2019). All of these proteins, plus many more, are needed to stabilize RFs and allow continuous DNA synthesis (Figure 6E, left).

Defects in assembling RAD51 filaments cause genomic instability (Kim et al., 2012); yet, we do not know the source of the genomic instability observed in these RAD51^{K133A} cells. Here, we show that TREX2's exonuclease activity caused most of the genomic instability for cells expressing RAD51^{K133A}, likely by degrading the nascent strand. We also show in cells deficient for PARP1 or mutant for FANCB that TREX2 protected the nascent strand independent of its exonuclease activity. To explain these paradoxical results, we present a model for two RF defects. First, a defect within the RAD51 filament that causes mutations as seen with RAD51^{K133A} and second, a general RF maintenance defect as seen with a PARP1 deficiency and a FANCB deletion.

First, we propose aberrant RAD51^{WT} and RAD51^{K133A} mixed filaments were more prone to degradation (Figure 6E, middle). This notion is supported by our observation that mixing RAD51^{K133A} with RAD51^{WT} failed to protect the strand from TREX2 exonuclease activity compared with RAD51^{WT} alone. TREX2's exonuclease activity was required to generate most of the mutations in RAD51^{K133A} cells since they were reduced by its deletion or expression of a catalytic defective TREX2. It is possible that TREX2's exonuclease activity was required to remove an obstacle such as a secondary structure involving the 3' terminus of the strand and that strand degradation ensued once it was removed. The secondary structure could be the filament with RAD51^{K133A}. These data are consistent with TREX2 performing a dual function (ubiquitinate PCNA and exonuclease activity).

Second, we propose that a general decline in RF maintenance due to either a PARP1 deficiency or a FANCB mutation resulted in nascent strand degradation (Figure 6E, right). This notion is supported by our observation that a PARP1 deficiency or FANCB mutation leads to a general decline in RF maintenance and that TREX2 protects the RF independent of its exonuclease activity. A possible function that protects the RF is PCNA ubiquitination, and this idea is supported by our data showing that TREX2^{H188A} was able to bind to UBC13 and ubiquitinate PCNA. These data are consistent with TREX2-mediated PCNA ubiquitination being uncoupled from TREX2-mediated strand degradation.

We propose that TREX2 caused spontaneous mutations in RAD51^{K133A}-expressing cells through the DDT pathway. This hypothesis is based on several previous observations that TREX2 participated in DDT by virtue of its *in vitro* and *in vivo* association with UBC13 and by the similarity of the null phenotypes for TREX2 and RAD18 including a defect in inverted mismatched repeat fusion, increased RF stalls, and inability to ubiquitinate PCNA (Hu et al., 2013). Here, we present another supportive feature since deletion of either TREX2 or RAD18 ablated most of the spontaneous mutations in RAD51^{K133A} cells. Furthermore, overexpression of PCNA^{WT} decreased the number of TG-resistant colonies, consistent with the notion that ubiquitinated PCNA is the key rate-limiting step. Failure to modify PCNA on K164 elevated the number of TG-resistant colonies. RAD18 and TREX2 ubiquitinate PCNA K164, a necessary step during

DDT (Hu et al., 2013; Kanao et al., 2015; Lee and Myung, 2008). Monoubiquitinated PCNA K164 initiates TLS, and many of the translesion polymerases are mutagenic (Jansen et al., 2015), while polyubiquitinated PCNA K164 initiates TS that can rearrange chromosomes when the strand anneals to a nonallelic template (Hu et al., 2013). TLS and TS likely occur in coordination to facilitate progression of the stalled fork and allow their restart to prevent RF collapse at the expense of increased risk of generating a mutation. Mutations could happen more frequently in mouse ESCs than most other cells due to their short G₁ phase that revealed frequent RF reversal along with massive ssDNA gap accumulation (Ahuja et al., 2016). Therefore, TREX2, RAD18, and unmodifiable PCNA K164 work in a common pathway to cause spontaneous mutations in HR-defective cells. An alternative explanation is that RFs are not reversed in RAD51^{K133A}-expressing cells when RAD18 is deleted perhaps due to dependency on PCNA polyubiquitination through recruitment of ZRANB3 (Zinc Finger Ran-binding Domain-containing Protein 3), a RF remodeler (Vujanovic et al., 2017), and as a consequence are not vulnerable to the deleterious effects of TREX2. By either explanation, we show that the defect in DDT will reduce the level of mutations or increase the level of cell death.

In conclusion, our data show that TREX2 deletion in RAD51^{K133A}-expressing cells reduced spontaneous mutations, RF stalls, nascent strand degradation, and PCNA ubiquitination. It also caused hypersensitivity to CPT and nascent strand degradation in PARP1-deficient and FANCB mutant cells. Interestingly, expression of TREX2^{WT} and TREX2^{H188A} rescued CPT hypersensitivity and stabilized the nascent strand in PARP1-deficient and FANCB mutant cells. Our results are consistent with TREX2 having a dual role that is either nuclease dependent or independent. The exonuclease-dependent outcome is to degrade the nascent strand with a faulty RAD51 filament, causing stalled RFs and genomic instability. The exonuclease-independent outcomes include UBC13 association and PCNA ubiquitination and could be essential for the phenotype observed in TREX2^{null} cells that are rescued by TREX2^{H188A}. Future steps include looking at the role of a variety of DNA repair pathways on RF maintenance when RAD51 and RAD51 paralog variants are expressed, including those associated with cancer and ones that disrupt a specific function.

STAR★METHODS

Detailed methods are provided in the online version of this paper and include the following:

- KEY RESOURCES TABLE
- RESOURCE AVAILABILITY
 - Lead Contact
 - Materials Availability
 - Data and Code Availability
- EXPERIMENTAL MODEL AND SUBJECT DETAILS
 - Cell Lines
- METHOD DETAILS
 - Targeting Trex2, Rad51, FancB and Top3β

- Generation of 3XFLAG-PCNA-RAD51 (WT, K133A) cells
- CRISPR/Cas9 mutation in Rad51^{+/3mH} cells
- Two-color FISH assay
- The miniHPRT LOF assay
- Chromosome painting on MPSs
- DNA fiber analysis
- Dose response curve
- Nuclease protection assay
- Protein purification
- iPOND (isolation of Proteins on Nascent DNA) assay
- TREX2^{H188A} pulldown with UBC13
- PCNA ubiquitination
- **QUANTIFICATION AND STATISTICAL ANALYSIS**

SUPPLEMENTAL INFORMATION

Supplemental Information can be found online at <https://doi.org/10.1016/j.celrep.2020.108543>.

ACKNOWLEDGMENTS

We thank Dr. Kyungjae Myung for the gift of 3XFLAG-PCNA^{WT} and 3XFLAG-PCNA^{K164R}, Dr. Thomas Hollis for TREX2 expression plasmid, Sherry Dodds for technical assistance, and the Molecular Cytogenetic Core at Albert Einstein College of Medicine—in particular Dr. Jidong Shan and Dr. Yinghui Song—for assisting with the two-color FISH studies. We also thank the Cryo-Electron Microscopy and Tomography Core Facility at CEITEC and appreciate access to computing and storage facilities of the National Grid Infrastructure MetaCentrum. This work was supported by the National Institutes of Health (USA) (1 R01 ES022054-04 to P.H. and 1 R01 CA188032-01 and 1 P01AG017242-17A1 to P.H. and C.M.), the Evans Foundation (USA), an IIMS pilot (USA) to P.H., and a postdoctoral training fellowship from the CPRIT research training award (RP170345) (USA) to M.Y.S. Research was also supported by the Albert Einstein Cancer Center Support Grant of the National Institutes of Health under award number P30CA013330. The work in Krejci's group was supported by Wellcome Trust (United Kingdom) collaborative grant 206292/E/17/Z; the Czech Science Foundation (GACR 17-17720S and 21-22593X) (Czechia); project LQ1605 from the National Program of Sustainability II (MEYS CR); Masaryk University [MUNI/G/1594/2019] and Operational Programme Research, Development and Education—Project Postdoc@MUNI (CZ.02.2.69/0.0/0.0/16_027/0008360).

AUTHOR CONTRIBUTIONS

P.H., L.K., and C.M. designed experiments and interpreted results. J.H.K., M.Y.S., Q.Z., L.M., L.S., J.M., A.J., and P.H. performed experiments. P.H., L.K., and C.M. wrote the paper with comments from the other authors.

DECLARATION OF INTERESTS

The authors declare no competing interests.

Received: October 16, 2019

Revised: April 23, 2020

Accepted: December 1, 2020

Published: December 22, 2020

REFERENCES

Ahuja, A.K., Jodkowska, K., Teloni, F., Bizard, A.H., Zellweger, R., Herrador, R., Ortega, S., Hickson, I.D., Altmeyer, M., Mendez, J., and Lopes, M. (2016). A short G1 phase imposes constitutive replication stress and fork remodeling in mouse embryonic stem cells. *Nat. Commun.* **7**, 10660.

Andriani, G.A., Almeida, V.P., Faggioli, F., Mauro, M., Tsai, W.L., Santambrogio, L., Maslov, A., Gadina, M., Campisi, J., Vijg, J., and Montagna, C. (2016). Whole Chromosome Instability induces senescence and promotes SASP. *Sci. Rep.* **6**, 35218.

Araki, K., Araki, M., and Yamamura, K. (1997). Targeted integration of DNA using mutant lox sites in embryonic stem cells. *Nucleic Acids Res.* **25**, 868–872.

Berti, M., Ray Chaudhuri, A., Thangavel, S., Gomathinayagam, S., Kenig, S., Vujanovic, M., Odreman, F., Glatter, T., Graziano, S., Mendoza-Maldonado, R., et al. (2013). Human RECQ1 promotes restart of replication forks reversed by DNA topoisomerase I inhibition. *Nat. Struct. Mol. Biol.* **20**, 347–354.

Bhat, K.P., and Cortez, D. (2018). RPA and RAD51: fork reversal, fork protection, and genome stability. *Nat. Struct. Mol. Biol.* **25**, 446–453.

Branzei, D., and Foiani, M. (2007). Template switching: from replication fork repair to genome rearrangements. *Cell* **131**, 1228–1230.

Branzei, D., and Psakhye, I. (2016). DNA damage tolerance. *Curr. Opin. Cell Biol.* **40**, 137–144.

Carr, A.M., and Lambert, S. (2013). Replication stress-induced genome instability: the dark side of replication maintenance by homologous recombination. *J. Mol. Biol.* **425**, 4733–4744.

Chen, P.-L., Chen, C.F., Chen, Y., Xiao, J., Sharp, Z.D., and Lee, W.H. (1998). The BRC repeats in BRCA2 are critical for RAD51 binding and resistance to methyl methanesulfonate treatment. *Proc. Natl. Acad. Sci. USA* **95**, 5287–5292.

Chen, M.J., Ma, S.M., Dumitrache, L.C., and Hasty, P. (2007). Biochemical and cellular characteristics of the 3' → 5' exonuclease TREX2. *Nucleic Acids Res.* **35**, 2682–2694.

Chi, P., Van Komen, S., Sehorn, M.G., Sigurdsson, S., and Sung, P. (2006). Roles of ATP binding and ATP hydrolysis in human Rad51 recombinase function. *DNA Repair (Amst.)* **5**, 381–391.

Choi, Y.J., Son, M.Y., and Hasty, P. (2011). One-step knockin for inducible expression in mouse embryonic stem cells. *Genesis* **49**, 92–97.

Dumitrache, L.C., Hu, L., and Hasty, P. (2009). TREX2 exonuclease defective cells exhibit double-strand breaks and chromosomal fragments but not Robertsonian translocations. *Mutat. Res.* **662**, 84–87.

Dumitrache, L.C., Hu, L., Son, M.Y., Li, H., Wesevich, A., Scully, R., Stark, J., and Hasty, P. (2011). Trex2 enables spontaneous sister chromatid exchanges without facilitating DNA double-strand break repair. *Genetics* **188**, 787–797.

Friedrich, G., and Soriano, P. (1991). Promoter traps in embryonic stem cells: a genetic screen to identify and mutate developmental genes in mice. *Genes Dev.* **5**, 1513–1523.

Fujihara, Y., and Ikawa, M. (2014). CRISPR/Cas9-based genome editing in mice by single plasmid injection. *Methods Enzymol.* **546**, 319–336.

Ghosal, G., and Chen, J. (2013). DNA damage tolerance: a double-edged sword guarding the genome. *Transl. Cancer Res.* **2**, 107–129.

Guenatri, M., Bailly, D., Maison, C., and Almouzni, G. (2004). Mouse centric and pericentric satellite repeats form distinct functional heterochromatin. *J. Cell Biol.* **166**, 493–505.

Hashimoto, K., Yonemori, K., Shimizu, C., Hirakawa, A., Yamamoto, H., Ono, M., Hirata, T., Kouno, T., Tamura, K., Katsumata, N., et al. (2010). A retrospective study of the impact of age on patterns of care for elderly patients with metastatic breast cancer. *Med. Oncol.* **28**, 434–440.

Hasty, P., Rivera-Pérez, J., Chang, C., and Bradley, A. (1991). Target frequency and integration pattern for insertion and replacement vectors in embryonic stem cells. *Mol. Cell Biol.* **11**, 4509–4517.

Hendel, A., Krijger, P.H., Diamant, N., Goren, Z., Langerak, P., Kim, J., Reissner, T., Lee, K.Y., Geacintov, N.E., Carell, T., et al. (2011). PCNA ubiquitination is important, but not essential for translesion DNA synthesis in mammalian cells. *PLoS Genet.* **7**, e1002262.

Holcomb, V.B., Kim, T.M., Dumitrache, L.C., Ma, S.M., Chen, M.J., and Hasty, P. (2007). HPRT minigene generates chimeric transcripts as a by-product of gene targeting. *Genesis* **45**, 275–281.

- Hu, L., Kim, T.M., Son, M.Y., Kim, S.A., Holland, C.L., Tateishi, S., Kim, D.H., Yew, P.R., Montagna, C., Dumitrache, L.C., and Hasty, P. (2013). Two replication fork maintenance pathways fuse inverted repeats to rearrange chromosomes. *Nature* *501*, 569–572.
- Huang, Y., Leung, J.W., Lowery, M., Matsushita, N., Wang, Y., Shen, X., Huang, D., Takata, M., Chen, J., and Li, L. (2014). Modularized functions of the Fanconi anemia core complex. *Cell Rep.* *7*, 1849–1857.
- Jansen, J.G., Tsaalbi-Shtylik, A., and de Wind, N. (2015). Roles of mutagenic translesion synthesis in mammalian genome stability, health and disease. *DNA Repair (Amst)* *29*, 56–64.
- Kanao, R., Masuda, Y., Deguchi, S., Yumoto-Sugimoto, M., Hanaoka, F., and Masutani, C. (2015). Relevance of simultaneous mono-ubiquitinations of multiple units of PCNA homo-trimers in DNA damage tolerance. *PLoS ONE* *10*, e0118775.
- Kim, T.M., Choi, Y.J., Ko, J.H., and Hasty, P. (2008). High-throughput knock-in coupling gene targeting with the HPRT minigene and Cre-mediated recombination. *Genesis* *46*, 732–737.
- Kim, D.H., Budhavarapu, V.N., Herrera, C.R., Nam, H.W., Kim, Y.S., and Yew, P.R. (2010). The CRL4Cdt2 ubiquitin ligase mediates the proteolysis of cyclin-dependent kinase inhibitor Xic1 through a direct association with PCNA. *Mol. Cell. Biol.* *30*, 4120–4133.
- Kim, T.M., Ko, J.H., Choi, Y.J., Hu, L., and Hasty, P. (2011). The phenotype of FancB-mutant mouse embryonic stem cells. *Mutat. Res.* *712*, 20–27.
- Kim, T.M., Ko, J.H., Hu, L., Kim, S.A., Bishop, A.J., Vijg, J., Montagna, C., and Hasty, P. (2012). RAD51 mutants cause replication defects and chromosomal instability. *Mol. Cell. Biol.* *32*, 3663–3680.
- Kolinjivadi, A.M., Crismani, W., and Ngeow, J. (2020). Emerging functions of Fanconi anemia genes in replication fork protection pathways. *Hum. Mol. Genet.* *29* (R2), R158–R164.
- Kondratova, A., Watanabe, T., Marotta, M., Cannon, M., Segall, A.M., Serre, D., and Tanaka, H. (2015). Replication fork integrity and intra-S phase checkpoint suppress gene amplification. *Nucleic Acids Res.* *43*, 2678–2690.
- Krejci, L., Altmanova, V., Spirek, M., and Zhao, X. (2012). Homologous recombination and its regulation. *Nucleic Acids Res.* *40*, 5795–5818.
- Krijger, P.H., Lee, K.Y., Wit, N., van den Berk, P.C., Wu, X., Roest, H.P., Maas, A., Ding, H., Hoeijmakers, J.H., Myung, K., and Jacobs, H. (2011). HLTf and SHPRH are not essential for PCNA polyubiquitination, survival and somatic hypermutation: existence of an alternative E3 ligase. *DNA Repair (Amst.)* *10*, 438–444.
- Lee, K.Y., and Myung, K. (2008). PCNA modifications for regulation of post-replication repair pathways. *Mol. Cells* *26*, 5–11.
- Liu, W., Zhou, M., Li, Z., Li, H., Polaczek, P., Dai, H., Wu, Q., Liu, C., Karanja, K.K., Popuri, V., et al. (2016). A Selective Small Molecule DNA2 Inhibitor for Sensitization of Human Cancer Cells to Chemotherapy. *EBioMedicine* *6*, 73–86.
- Marini, V., and Krejci, L. (2012). Unwinding of synthetic replication and recombination substrates by Srs2. *DNA Repair (Amst.)* *11*, 789–798.
- Mazur, D.J., and Perrino, F.W. (1999). Identification and expression of the TREX1 and TREX2 cDNA sequences encoding mammalian 3'→5' exonucleases. *J. Biol. Chem.* *274*, 19655–19660.
- Mazur, D.J., and Perrino, F.W. (2001). Excision of 3' termini by the Trex1 and TREX2 3'→5' exonucleases. Characterization of the recombinant proteins. *J. Biol. Chem.* *276*, 17022–17029.
- McCulloch, S.D., and Kunkel, T.A. (2008). The fidelity of DNA synthesis by eukaryotic replicative and translesion synthesis polymerases. *Cell Res.* *18*, 148–161.
- Meetei, A.R., Levitus, M., Xue, Y., Medhurst, A.L., Zwaan, M., Ling, C., Roovers, M.A., Bier, P., Hoatlin, M., Pals, G., et al. (2004). X-linked inheritance of Fanconi anemia complementation group B. *Nat. Genet.* *36*, 1219–1224.
- Meuth, M. (1989). The molecular basis of mutations induced by deoxyribonucleoside triphosphate pool imbalances in mammalian cells. *Exp. Cell Res.* *181*, 305–316.
- Mijic, S., Zellweger, R., Chappidi, N., Berti, M., Jacobs, K., Mutreja, K., Ursich, S., Ray Chaudhuri, A., Nussenzweig, A., Janscak, P., and Lopes, M. (2017). Replication fork reversal triggers fork degradation in BRCA2-defective cells. *Nat. Commun.* *8*, 859.
- Montague, T.G., Cruz, J.M., Gagnon, J.A., Church, G.M., and Valen, E. (2014). CHOPCHOP: a CRISPR/Cas9 and TALEN web tool for genome editing. *Nucleic Acids Res.* *42*, W401–W407.
- Motegi, A., Liaw, H.J., Lee, K.Y., Roest, H.P., Maas, A., Wu, X., Moinova, H., Markowitz, S.D., Ding, H., Hoeijmakers, J.H., and Myung, K. (2008). Polyubiquitination of proliferating cell nuclear antigen by HLTf and SHPRH prevents genomic instability from stalled replication forks. *Proc. Natl. Acad. Sci. USA* *105*, 12411–12416.
- Perrino, F.W., Harvey, S., McMillin, S., and Hollis, T. (2005). The human TREX2 3'→5' exonuclease structure suggests a mechanism for efficient nonprocessive DNA catalysis. *J. Biol. Chem.* *280*, 15212–15218.
- Petermann, E., Orta, M.L., Issaeva, N., Schultz, N., and Helleday, T. (2010). Hydroxyurea-stalled replication forks become progressively inactivated and require two different RAD51-mediated pathways for restart and repair. *Mol. Cell* *37*, 492–502.
- Pilzecker, B., Buoninfante, O.A., and Jacobs, H. (2019). DNA damage tolerance in stem cells, ageing, mutagenesis, disease and cancer therapy. *Nucleic Acids Res.* *47*, 7163–7181.
- Prakash, S., Johnson, R.E., and Prakash, L. (2005). Eukaryotic translesion synthesis DNA polymerases: specificity of structure and function. *Annu. Rev. Biochem.* *74*, 317–353.
- Rajendra, E., Oestergaard, V.H., Langevin, F., Wang, M., Dornan, G.L., Patel, K.J., and Passmore, L.A. (2014). The genetic and biochemical basis of FANCD2 monoubiquitination. *Mol. Cell* *54*, 858–869.
- Rickman, K., and Smogorzewska, A. (2019). Advances in understanding DNA processing and protection at stalled replication forks. *J. Cell Biol.* *218*, 1096–1107.
- Roy, R., Chun, J., and Powell, S.N. (2011). BRCA1 and BRCA2: different roles in a common pathway of genome protection. *Nat. Rev. Cancer* *12*, 68–78.
- San Filippo, J., Chi, P., Sehorn, M.G., Etchin, J., Krejci, L., and Sung, P. (2006). Recombination mediator and Rad51 targeting activities of a human BRCA2 polypeptide. *J. Biol. Chem.* *281*, 11649–11657.
- Schlacher, K., Christ, N., Siaud, N., Egashira, A., Wu, H., and Jasin, M. (2011). Double-strand break repair-independent role for BRCA2 in blocking stalled replication fork degradation by MRE11. *Cell* *145*, 529–542.
- Schlacher, K., Wu, H., and Jasin, M. (2012). A distinct replication fork protection pathway connects Fanconi anemia tumor suppressors to RAD51-BRCA1/2. *Cancer Cell* *22*, 106–116.
- Schneider, C.A., Rasband, W.S., and Eliceiri, K.W. (2012). NIH Image to ImageJ: 25 years of image analysis. *Nat. Methods* *9*, 671–675.
- Sharan, S.K., Morimatsu, M., Albrecht, U., Lim, D.S., Regel, E., Dinh, C., Sands, A., Eichele, G., Hasty, P., and Bradley, A. (1997). Embryonic lethality and radiation hypersensitivity mediated by Rad51 in mice lacking Brca2. *Nature* *386*, 804–810.
- Sigurdsson, S., Van Komen, S., Bussen, W., Schild, D., Albala, J.S., and Sung, P. (2001). Mediator function of the human Rad51B–Rad51C complex in Rad51/RPA-catalyzed DNA strand exchange. *Genes Dev.* *15*, 3308–3318.
- Sirbu, B.M., Couch, F.B., Feigerle, J.T., Bhaskara, S., Hiebert, S.W., and Cortez, D. (2011). Analysis of protein dynamics at active, stalled, and collapsed replication forks. *Genes Dev.* *25*, 1320–1327.
- Sirbu, B.M., Couch, F.B., and Cortez, D. (2012). Monitoring the spatiotemporal dynamics of proteins at replication forks and in assembled chromatin using isolation of proteins on nascent DNA. *Nat. Protoc.* *7*, 594–605.
- Sogo, J.M., Lopes, M., and Foiani, M. (2002). Fork reversal and ssDNA accumulation at stalled replication forks owing to checkpoint defects. *Science* *297*, 599–602.
- Son, M.Y., and Hasty, P. (2019). Homologous recombination defects and how they affect replication fork maintenance. *AIMS Genet.* *5*, 192–211.

- Špírek, M., Mlcousková, J., Belán, O., Gyimesi, M., Harami, G.M., Molnár, E., Novacek, J., Kovács, M., and Krejci, L. (2018). Human RAD51 rapidly forms intrinsically dynamic nucleoprotein filaments modulated by nucleotide binding state. *Nucleic Acids Res.* *46*, 3967–3980.
- Taniguchi, T., Garcia-Higuera, I., Andreassen, P.R., Gregory, R.C., Grompe, M., and D'Andrea, A.D. (2002). S-phase-specific interaction of the Fanconi anemia protein, FANCD2, with BRCA1 and RAD51. *Blood* *100*, 2414–2420.
- Tao, S.S., Wu, G.C., Zhang, Q., Zhang, T.P., Leng, R.X., Pan, H.F., and Ye, D.Q. (2019). TREX1 As a Potential Therapeutic Target for Autoimmune and Inflammatory Diseases. *Curr. Pharm. Des.* *25*, 3239–3247.
- Vaz, F., Hanenberg, H., Schuster, B., Barker, K., Wiek, C., Erven, V., Neveling, K., Endt, D., Kesterton, I., Autore, F., et al. (2010). Mutation of the RAD51C gene in a Fanconi anemia-like disorder. *Nat. Genet.* *42*, 406–409.
- Vujanovic, M., Krietsch, J., Raso, M.C., Terraneo, N., Zellweger, R., Schmid, J.A., Tagliatela, A., Huang, J.W., Holland, C.L., Zwicky, K., et al. (2017). Replication Fork Slowing and Reversal upon DNA Damage Require PCNA Polyubiquitination and ZRANB3 DNA Translocase Activity. *Mol. Cell* *67*, 882–890.e885.
- Wang, W. (2007). Emergence of a DNA-damage response network consisting of Fanconi anaemia and BRCA proteins. *Nat. Rev. Genet.* *8*, 735–748.
- Zellweger, R., Dalcher, D., Mutreja, K., Berti, M., Schmid, J.A., Herrador, R., Vindigni, A., and Lopes, M. (2015). Rad51-mediated replication fork reversal is a global response to genotoxic treatments in human cells. *J. Cell Biol.* *208*, 563–579.

STAR★METHODS

KEY RESOURCES TABLE

REAGENT or RESOURCE	SOURCE	IDENTIFIER
Antibodies		
Rat monoclonal anti-BrdU [BU1/75 (ICR1)]	AbD Serotec (Bio-Rad)	Cat# MCA2060T; RRID:AB_10015293
Mouse monoclonal anti-BrdU (B44)	BD Biosciences	Cat# 347580; RRID:AB_10015219
Goat anti-rat AlexaFluor555	Thermo Fisher	Cat# A-21434; RRID:AB_141733
Goat anti-mouse AlexaFluor488	Thermo Fisher	Cat# A-11017; RRID:AB_143160
Rabbit anti-Rad51 (H-92)	Santa Cruz Biotechnology	Cat# SC-8349; RRID:AB_2253533
Mouse anti-PCNA (PC-10)	Santa Cruz Biotechnology	Cat# SC-56; RRID:AB_628110
Mouse monoclonal anti-FLAG (M2)	Sigma-Aldrich	Cat# F1804; RRID:AB_262044
Rabbit polyclonal anti-Histone H3 (C-16)	Santa Cruz Biotechnology	Cat# SC-8654; RRID:AB_2118303
Mouse monoclonal anti-Ubiquitin (P4D1)	Covance	Cat# MMS-257P-200; RRID:AB_291363
Mouse TrueBlot ULTRA: Anti-Mouse Ig HRP	Rockland-Inc	Cat# 18-8817-30; RRID:AB_2610849
IRDye 680RD goat anti-rabbit	Li-COR Biosciences	Cat# 926-68071; RRID:AB_10956166
IRDye 800CW goat anti-mouse	Li-COR Biosciences	Cat# 926-32210; RRID: AB_621842
Chemicals, Peptides, and Recombinant Proteins		
Lipofectamine 3000	Thermo Fisher-Invitrogen	Cat# L30000001
Camptothecin	Sigma-Aldrich	Cat# C9911
Hydroxyurea	Sigma-Aldrich	Cat# H8627
Mirin	Sigma-Aldrich	Cat# M9948
DNA2 inhibitor C5	AOBIOUS	Cat# AOB9082
Olaparib	Selleckchem	Cat# S1060
Colcemid	Santa Cruz	Cat# SC-202550
Vectashield mounting medium with DAPI	Vector Laboratories	Cat# H-1200
Formamide	Fisher Scientific	Cat# BP227-500
CldU (5'-Chloro-2'-deoxyuridine)	Sigma-Aldrich	Cat# C6891
IdU (5-Iodo-2'-deoxyuridine)	Sigma-Aldrich	Cat# I7125
Paraformaldehyde	Electron Microscopy Sciences	Cat#15710
cOmplete mini protease inhibitor cocktail	Roche	Cat# 11836170001
50x HAT	Sigma-Aldrich	Cat# H0262
50x HT	Sigma-Aldrich	Cat# H0137
6-Thioguanine	Sigma-Aldrich	Cat# A4882
DMSO (dimethyl sulfoxide)	Sigma-Aldrich	Cat# D2650
EdU (5-ethynyl-2'-deoxyuridine)	Invitrogen	Cat# E10187
Formaldehyde	Sigma-Aldrich	Cat# F8775
Biotin-azide	Invitrogen	Cat# C10269
Streptavidin-agarose	Novagen	Cat# 69203-3
Doxycycline	Clonetech	Cat# 631311
Orange 552 dUTP (lyophilized)	Enzo	Cat # ENZ-42842L-0050
Spectrum green mouse chromosome 2 painting probe	Applied Spectral Imaging	Cat# PRPR0169/M10

(Continued on next page)

Continued

REAGENT or RESOURCE	SOURCE	IDENTIFIER
Antifade 4,6-diamidino-2-phenylindole (DAPI) – Vial no 5	Applied Spectral Imaging	Cat# FPRPR0006
Experimental Models: Cell Lines		
Mouse: AB2.2 Trex2 ^{WT} RAD51 ^{WT}	This paper	N/A
Mouse: AB2.2 Trex2 ^{null} RAD51 ^{WT}	This paper	N/A
Mouse: AB2.2 Trex2 ^{H188A} RAD51 ^{WT}	This paper	N/A
Mouse: AB2.2 Trex2 ^{WT} RAD51 ^{K133A}	This paper	N/A
Mouse: AB2.2 Trex2 ^{null} RAD51 ^{K133A}	This paper	N/A
Mouse: AB2.2 Trex2 ^{H188A} RAD51 ^{K133A}	This paper	N/A
Mouse: AB2.2 RAD18 ^{+/+} RAD51 ^{K133A}	This paper	N/A
Mouse: AB2.2 RAD18 ^{-/-} RAD51 ^{K133A}	This paper	N/A
Mouse: AB2.2 RAD18 ^{+/+} RAD51 ^{K133A} NT	This paper	N/A
Mouse: AB2.2 RAD18 ^{+/+} RAD51 ^{K133A} dox	This paper	N/A
Mouse: AB2.2 RAD18 ^{-/-} RAD51 ^{WT} NT	This paper	N/A
Mouse: AB2.2 RAD18 ^{-/-} RAD51 ^{K133A} dox	This paper	N/A
Mouse: AB2.2 EV RAD51 ^{WT}	This paper	N/A
Mouse: AB2.2 PCNA ^{WT} RAD51 ^{WT}	This paper	N/A
Mouse: AB2.2 PCNA ^{K164R} RAD51 ^{WT}	This paper	N/A
Mouse: AB2.2 EV RAD51 ^{K133A}	This paper	N/A
Mouse: AB2.2 PCNA ^{WT} RAD51 ^{K133A}	This paper	N/A
Mouse: AB2.2 PCNA ^{K164R} RAD51 ^{K133A}	This paper	N/A
Mouse: AB2.2 TREX2 ^{WT} FB ^{WT}	This paper	N/A
Mouse: AB2.2 TREX2 ^{null} FB ^{WT}	This paper	N/A
Mouse: AB2.2 TREX2 ^{H188A} FB ^{WT}	This paper	N/A
Mouse: AB2.2 TREX2 ^{WT} FB ^{MUT}	This paper	N/A
Mouse: AB2.2 TREX2 ^{null} FB ^{MUT}	This paper	N/A
Mouse: AB2.2 TREX2 ^{H188A} FB ^{MUT}	This paper	N/A
Mouse: AB2.2 mTREX2 ^{WT}	Chen et al., 2007	N/A
Mouse: AB2.2 TREX2 ^{null}	Chen et al., 2007	N/A
Mouse: AB2.2 hTREX2 ^{WT}	Chen et al., 2007	N/A
Mouse: AB2.2 TREX2 ^{H188A}	Chen et al., 2007	N/A
Oligonucleotides		
Rad18 gRNAe1F: 5'-CACCGAGTCTGCGCCGAGCCGCGA-3'	This study	N/A
Rad18 gRNAe1R: 5'-AAACTCGCGGCTCGGCCAGGACCTC-3'	This study	N/A
Rad18 4DF: 5'-GGATGCTTACAGAAAGAGGAG-3'	This study	N/A
Rad18 3DR: 5'-CGTTGACACTACTTTACGGG-3'	This study	N/A
mTop3β Cre screen For2: 5'-TCACAGAGTTCTCTGAGCATTGG-3'	This study	N/A
RCF1 (in mouse RAD51 intron1): 5'-GTGCTGAATCTCCTAGAACTG-3'	Kim et al., 2012	N/A
hPCNA rev1: 5'-ACTAGCGCCAAGGTATCCGCG-3'	This study	N/A
bpA rev2: 5'-AGAACGGTCCGCCGCATCC-3'	This study	N/A
HsMmPCNA For: 5'-CTGCSGSGCSTGGSCCTCGTC-3'	This study	N/A
FDR: 5'-AGCATGCTGACAATGACTGC-3'	Kim et al., 2008	N/A
Recombinant DNA		
pX330-U6-Chimeric_BB-CBh-hSpCas9	Addgene	RRID:Addgene_42230
pPGKcrepA	Kim et al., 2008	N/A
pCAGGS-FLPe	Kim et al., 2008	N/A
CMKIP-RAD51cDNA(WT)	Kim et al., 2012	N/A
CMKIP-RAD51cDNA(K133A)	Kim et al., 2012	N/A

(Continued on next page)

Continued

REAGENT or RESOURCE	SOURCE	IDENTIFIER
hTrex2WT	Chen et al., 2007	N/A
hTrex2KS	Chen et al., 2007	N/A
hTrex2CD	Chen et al., 2007	N/A
Tet-Puro-RAD51WT	This study	N/A
Tet-Puro-RAD51K133A	This study	N/A
3xFLAG-hPCNAWT	This study	N/A
3xFLAG-hPCNAK164R	This study	N/A
3xFLAG-hPCNAEV	This study	N/A
FancB	Kim et al., 2011	N/A
BAC clone RP23-131B18	Children's Hospital, Okalanda, CA	N/A

Software and Algorithms

Zen 2.3 pro	Zeiss	RRID:SCR_013672
Prism8	GraphPad	RRID:SCR_002798
Odyssey Infrared Imaging System Image studio version 3.0 software	Li-COR Biosciences	RRID:SCR_013715
GenASIs software Version 8.1	Applied Spectral Imaging	N/A
Multi Gauge V3.2	Fujifilm	N/A
ImageJ	Schneider et al., 2012	RRID:SCR_003070

RESOURCE AVAILABILITY

Lead Contact

Correspondence and requests for materials should be addressed to and will be fulfilled by the Lead Contact, Paul Hasty (hastye@uthscsa.edu).

Materials Availability

Plasmids and cell lines generated in this study are available by request and will be fulfilled by the Lead Contact, Paul Hasty (hastye@uthscsa.edu).

Data and Code Availability

This study did not generate datasets or code.

EXPERIMENTAL MODEL AND SUBJECT DETAILS

Cell Lines

The cell culture conditions for mouse embryonic stem cells (AB2.2 - XY ES cells) have been described ([Hasty et al., 1991](#)). The cells were cultured in Dulbecco's Modified Eagle's Medium (DMEM) with 15% fetal bovine serum (Gemini Bio), 2 mM glutamine, 30 ug/mL penicillin, 50 ug/mL streptomycin, 10^{-4} M β -mercaptoethanol (Sigma-Aldrich), and 1000 units/mL 10^7 mouse leukemia inhibitory factor (GeminiBio). The cells were cultured on cell culture dishes coated with 0.1% gelatin. The cells were maintained at 37°C in a 5% CO₂ humidified incubator. Cell lines are maintained at low passage number (≤ 10), but have not been authenticated.

METHOD DETAILS

Targeting *Trex2*, *Rad51*, *FancB* and *Top3 β*

The knockout-knockin protocol has been described for *Trex2* except the targeting vector used here contained the *MmTrex2* cDNA 5' to *miniHPRT* ([Dumitrache et al., 2009](#)). The knockout-knockin protocol has been described for *Rad51* ([Kim et al., 2012](#)) and for *Top3 β* ([Kim et al., 2008](#)). The knockin for the inducible system has been described for *Top3 β* but, here it is applied to *Rad51* ([Choi et al., 2011](#)). The *FancB* knockout ([Kim et al., 2011](#)) and the *Rad51* knockins have been described ([Kim et al., 2012](#)).

Generation of 3XFLAG-PCNA-RAD51 (WT, K133A) cells

Knock-in vectors for 3XFLAG-PCNA [WT, null (empty vector), K164R] were transfected in *Top3 β ^{+/-} Rad51^{+/-3mH}* cells by electroporation, cultured in 1xHAT medium. HAT-resistant colonies were picked and expanded and DNA was isolated for PCR. PCR screening

was used to detect the presence of 3XFLAG-PCNA (WT, K164R) knock-in using primers: *Top3β* Cre screen for2 (5'-TCACA-GAGTTCTCTGAGCATTGG-3') or RCF1 (in mouse *RAD51* intron 1; 5'-GTGCTGAATCTCCTAGAAGT-3') and hPCNA rev1 (5'-AC-TAGCGCCAAGGTATCCGCG-3'). The PCR conditions were 1 cycle of 98°C for 5 min, followed by 35 cycles of 98°C for 1 min, 66°C or 62°C for 1 min, and 72°C for 45 s, followed by 1 cycle of 72°C for 10 min. Knock-in colonies of 3XFLAG-PCNA (WT, K164R) located to *Top3β* loci (WT-18 & K164R-3, -5) were verified by iPOND (Figure 5C). The following primers were used to detect PCNA null (empty vector) knock-in: *Top3β* Cre screen for2 or RCF1 and bpA rev2 (5'-AGAACGGTCCGCCGCATCC-3'). The PCR conditions were 1 cycle of 98°C for 5 min, followed by 32 cycles of 98°C for 1 min, 66°C or 62°C for 1 min, and 72°C for 30 s, followed by 1 cycle of 72°C for 10 min. To remove *miniHPRT* and the plasmid backbone, flip recombinase was transfected into the 3XFlag-PCNA (WT, null, K164R) *Rad51^{+/-3mH}* cells with lipofectamine-3000. These cells were selected in 1xTG medium for 7-10 days. TG-resistant colonies were picked and screened by PCR using primers: HsMmPCNA for (5'-CTGCAGAGCATGGACTCGTC-3') and FDR (5'-AGCATGCTGACAATGACTGC-3'), PCR conditions: 35 cycles of 98°C for 1 min, 53°C for 1 min, and 67°C for 30 s, followed by 1 cycle of 72°C for 10 min. Positive clones were detected with a 1 kb band. The following PCRs were performed to distinguish 3XFlag-PCNA WT and K164R from null. To detect 3XFlag-PCNA WT and K164R the following primers were used: mTop3b Cre screen for2 and FDR. The PCR conditions were 35 cycles of 98°C for 1 min, 53°C for 1 min, and 67°C for 45 s, followed by 1 cycle of 72°C for 10 min. A 1.5kb band was observed if *miniHPRT* and the plasmid backbone was removed for 3XFlag-PCNA WT and K164R but no band would be observed for 3XFlag-PCNA null. The following was done to generate knockin of *Rad51* (WT, K133A). Electroporation was used to knockin *Rad51* (WT, K133A) vectors into cells. Transfected cells were selected in 1xHAT medium for 7-10 days. HAT-resistant colonies were picked and genomic DNA was isolated for PCR as described (Kim et al., 2012).

CRISPR/Cas9 mutation in *Rad51^{+/-3mH}* cells

CHOPCHOP (Montague et al., 2014) was used to design the *Rad18* gRNA plasmids that were inserted into the pX330 vector (Fujihara and Ikawa, 2014). These gRNA plus Cre recombinase (300 ng each) was transfected into *Rad51^{+/-3mH}* cells (described in Figure 1A) with the full length of *miniHPRT* (1x10⁴/well) with lipofectamine3000. Three days later the cells were transferred to a 10 cm plate with TG selection media to select for cells that have removed the 5' half of *miniHPRT* and subsequently for cells that took up the gRNA. Pick TG-resistant colonies 7-10 days later. The *Rad18* gRNA was located in exon 1 (CACCGAGGTCCTGGCCGAGCCGCGA). A positive colony was obtained by PCR screening using the 4DF and 3DR primers: 4DF: 5' GGATGCTTACAGAAAGAGGAG 3' and 3DR: 5' CGTTGACACTACTTTACGGG 3'. PCR conditions: 1 cycle of 98°C for 5 min, followed by 35 cycles of 98°C for 1 min, 62°C for 1 min, and 72°C for 15 s, followed by 1 cycle of 72°C for 6 min. This PCR fragment was sequenced and the entire coding sequence found in exon 1 was deleted.

Two-color FISH assay

This experiment has been described previously (Kim et al., 2012). The cells were incubated with 1 μg/mL of colcemid for 4 hr. The cells were harvested, resuspended with prewarmed 60 mM KCl and incubated at 37°C for 15 min. The cells were fixed in methanol and acetic acid (2:1). The cells were dropped onto microscope slides (Thermo scientific). The slides were air-dried and aged in 100% methanol for overnight. The slides were incubated with 70% formamide in 2x SSC buffer (3 M NaCl, 0.3 M sodium citrate) at 72°C for 10 min. The slides were incubated with 30% formamide, 0.27 μg/mL major satellite repeat probe (CY-3 5'-TGGAATATGGCGA-GAAAAGTAAAATCATGGAAAATGAGA-3') and telomeric probe (6-FAM 5'-(CCCTAA)7-3') in 2x SSC buffer at 37°C for 25 min. The slides were washed with 2x SSC buffer ten times and mounted using Vectashield mounting medium with DAPI (Vector Laboratories). The images were captured with Axio Imager A2 at 63x magnification (Zeiss) and analyzed with Zen 2.3pro software (Zeiss). At least 60 MPSs were scored and analyzed.

The *miniHPRT* LOF assay

The conditions for this experiment have been described (Kim et al., 2012) with modifications. The cells were kept in 1x HAT for 2 days, followed by kept in 1x HT for 3 days and then only fresh medium for 1 day. Next day, the cells were seeded at 2x10⁵/10 cm feeder plate (3 plates) with 10 μM 6-TG. For plating efficiency, the cells were seeded at 2x10³/two wells of 6-well feeder plate. The number of colonies were counted at day 7. For Figure 5B, the cells were kept in 2 μg/mL doxycycline for 10 days and then followed as above. The experiments were performed at least three times.

Chromosome painting on MPSs

FISH was used for the analysis of structural alterations mapping to chromosome 2 with two different probes: a chromosome 2 paint probe and a distal randomly selected locus specific probe mapping to chr2:160,089,813-160,314,595 (NCBI37/mm9). The bacterial artificial chromosome (BAC) clone RP23-131B18, mapping to chromosome 2 qH2, was obtained from the Children's Hospital, Oakland, CA. This probe was labeled via nick translation using DY-590-dUTP (Dyomics, Jena, GE) as previously described (Andriani et al., 2016) and combined 1:1 with a spectrum green mouse chromosome 2 painting probe (Applied Spectral Imaging, Carlsbad, CA). Metaphase chromosomes were prepared using standard methods. Briefly, cell suspensions were pelleted and incubated with hypotonic KCl solution (0.075 M KCl pre-warmed at 37°C, ThermoFisher). The cells were then fixed and washed four times with methanol/acetic acid solution (3:1). 40 μL of the cell suspension was dropped onto a clean slide, in 48% humidity and 24°C, and then stored at 37°C until analyzed. Probes were applied onto the slides, covered with the square coverslips and incubated over-

night at 37°C in a humidified chamber. After washing 3 times with 50% formamide/2x SSC for 5 min and three times with 1x SSC for 5 min, the slides were counterstained with 4,6-diamidino-2-phenylindole (DAPI) for 10 min and dehydrated with ethanol series and analyzed at 40X magnification using an Axiovert 200 (Zeiss) and the GenASIs (Version 8.1) software (Applied Spectral Imaging).

DNA fiber analysis

For replication fork stalling, this experiment has been described previously (Kim et al., 2012). The cells were pulsed with 25 μ M IdU for 20 min, washed with medium three times, and treated with 0.5 mM HU for 1.5 hr. The cells were washed with medium three times and pulsed with 250 μ M CldU for 20 min. Then, the cells were washed with ice-cold PBS twice, harvested and mixed with unlabeled cells (1:10). To prepare DNA fiber spreads, 2.5 μ L of cells were dropped onto microscope slides (Thermo scientific) and dried for 6 min. Then, the cells were lysed with 7.5 μ L of spreading buffer (200 mM Tris-HCl pH 7.4), 50 mM EDTA, 0.5% SDS) and incubated for 2 min. The slides were tilted at 15° and the DNA fibers were spread slowly down to the slides. The DNA fibers were fixed in methanol/acetic acid (3:1) for 10 min and air-dried. The DNA fibers were washed with ddH₂O for 5 min twice, rinsed with 2.5 M HCl for 2 min, and denatured in 2.5 M HCl for 1.25 hr. The fibers were rinsed with PBS twice and washed with blocking buffer (1% BSA, 0.1% Tween 20 in PBS) for 5 min twice. The fibers were incubated in blocking buffer for 0.5 hr and followed by incubation with rat α -BrdU (1:650) and mouse α -BrdU (1:650) in blocking buffer for 1 hr. The fibers were rinsed with PBS three times and fixed in 4% paraformaldehyde for 10 min. After rinses with PBS and washes with blocking buffer three times, the slides were incubate with secondary antibodies (anti-rat AlexaFluor 555 and anti-mouse AlexaFluor 488, 1:500) for 1.5 hr. The slides were rinsed with PBS twice, washed with blocking buffer three times and rinsed with PBS twice. Then, the slides were mounted with Fluoroshield (Sigma-Aldrich). DNA fibers were captured with Axio Imager A2 at 63x magnification (Zeiss) and analyzed using Zen 2.3pro software (Zeiss). At least 500 fibers for replication fork stalling were counted and analyzed. For nascent DNA degradation, the cells were pulsed with 25 μ M IdU for 30 min, washed with medium three times, pulsed with 250 μ M CldU for 30 min, washed with medium three times and treated 4 mM HU with or without 50 μ M mirin or 20 μ M C5 for 5 hr. For nascent DNA degradation with PARP inhibition, the cells were treated with 10 μ M olaparib for 2 hr. Then, the cells were pulsed with 25 μ M IdU and 250 μ M CldU with olaparib. Next, the cells were treated with 4 mM HU for 5 hr. The next procedures were described above. At least 100 fibers were counted and analyzed.

Dose response curve

For the colony-forming assay on day 0, 5×10^3 cells were seeded onto a 10 cm plate. On day1, cells were treated with CPT (15, 30, 60, 90, 120 nM). On day 8, colonies were washed with PBS and stained with 0.2% methylene blue in 70% ethanol and then counted. The experiment was performed three times.

Nuclease protection assay

A 5-fluorescein-labeled 30-mer ssDNA was annealed to 65-mer ssDNA containing phosphorothioate bonds as described previously (Marini and Krejci, 2012). RAD51^{WT} or RAD51^{K133A} proteins were pre-incubated with 20 nM 5-fluorescein-labeled DNA substrate (30-mer + 65-mer) in buffer containing 25 mM Tris-HCl [pH 7.5], 10 mM KCl, 1 mM DTT, 100 μ g/mL BSA, 2 mM MgCl₂ and 2 mM ATP for 5 min at 37°C, followed by addition of 450 nM TREX2 and incubation at 37°C for 30 minutes. The samples were deproteinized with 0.125% SDS and 500 μ g/mL of proteinase K at 37°C for 5 min, heat-denatured and resolved on a denaturing 15% polyacrylamide gel. Gels were imaged on a FLA 9000 scanner (Fujifilm) and quantified using Multi Gauge V3.2 software (Fujifilm). The amount of DNA degraded was quantified for all samples and then normalized to the initial amount of substrate, which was considered as 100% protected DNA. The protocol for the mixed filaments was the same, except that RAD51^{WT} and RAD51^{K133A} were incubated together for 3 min at room temperature prior adding to 5' fluorescently labeled DNA substrate.

Protein purification

Human RAD51^{WT} and K133A were overexpressed in bacterial cells and purified according to the previously published protocol (Špírek et al., 2018). Briefly, the proteins were purified by ammonium sulfate precipitation (0.242 mg/mL) followed by chromatography on Q Sepharose Fast Flow column (GE Healthcare), hydroxyapatite column (Sigma-Aldrich) and Mono Q column (GE Healthcare). Peak fractions containing RAD51 proteins were pooled, concentrated and stored at -80°C. Human TREX2 gene was expressed as a fusion with the maltose binding protein (MBP) in pLM303, a pET-27b derivative encoding a polyhistidine sequence on the N terminus of MBP and a rhinovirus 3C protease recognition site between the MBP and TREX2 genes. Expression plasmid MBP-TREX2 was introduced into BL21 (DE3) strain of *Escherichia coli* for overexpression. The cells were grown to an OD 0.7 at 37°C in 2 \times TY media supplemented with kanamycin, then shifted to at 16°C and expression was induced overnight with 0.5 mM IPTG. The bacterial pellet was resuspended in cell breakage buffer (CBB) (50 mM Tris-HCl pH 7.5, 10% sucrose, 0.5 mM EDTA, 300 mM KCl, 0.01% NP-40, cocktail of protease inhibitors, and PMSF), sonicated and centrifuged at 100,000 \times g for 1 hr. The clarified supernatant was incubated with Amylose Resin High Flow (New England Biolabs) pre-equilibrated in CBB buffer for 2 hr at 4°C. To release the TREX2 protein from Amylose resin and remove the MBP tag from the fusion, T buffer (25 mM Tris-HCl pH 7.5, 10% glycerol, 0.5 mM EDTA, and 0.01% NP-40) supplemented with 300 mM KCl and 5–25 μ g PreScission Protease was added to the beads and incubated overnight on a rotary shaker at 4°C. Eluted TREX2 protein fraction was loaded onto a hydroxyapatite (Sigma-Aldrich) column equilibrated with T buffer containing 100 mM KCl and 1 mM DTT. TREX2 protein was eluted by linear gradient of 0-700 mM KH₂PO₄ gradient in T buffer. Pooled peak fractions were loaded on Mono Q column (GE Healthcare) equilibrated with T buffer with

100 mM KCl and 1 mM DTT. TREX2 protein was eluted with 0–800 mM KCl gradient in T buffer. The fractions containing TREX2 protein were pooled, concentrated and stored at -80°C .

iPOND (isolation of Proteins on Nascent DNA) assay

Cells ($\sim 5 \times 10^7$ cells per sample) were incubated with 10 mM EdU for 1.5 hr. EdU-labeled cells were washed once, cells were cross-linked in 1% formaldehyde in PBS for 20 min at room temperature, quenched using 0.125 M glycine, and washed three times in PBS. Collected cell pellets were frozen at 80°C , then resuspended in 0.25% Triton-X/PBS to permeabilize. Pellets were washed once with 0.5% BSA/PBS and once with PBS prior to the click reaction. Cells were incubated in click reaction buffer containing 10 μM biotin-azide, 10 mM Na ascorbate, 2 μM CuSO_4 in PBS for 1.5 hr at a concentration of 1×10^7 cells per milliliter of click reaction buffer. DMSO was added instead of biotin-azide to the negative control samples (NC in the figure). Cell pellets were washed once with 0.5% BSA/PBS and once with PBS. Cell lysis Cells were then resuspended in lysis buffer containing 1% SDS, 50 mM Tris (pH 8.0), 1x protease inhibitor in 1 mL H_2O . Samples were sonicated on ice (120 Sonic Dismembrator, Fisher Scientific) using the following settings: 45% amplitude, 20 s constant pulse, and 40- sec pause for a total of 5 min. Samples were centrifuged at 16000 rpm for 10 min and diluted 1:1 (v/v) with PBS containing protease inhibitor prior to purification. Streptavidin-agarose beads were washed 1:1 (v/v) twice in lysis buffer and once in PBS. Washed beads were incubated with the samples for 14–20 hr at 4°C in the dark. The beads were washed once with lysis buffer, once with 1 M NaCl, and then twice with lysis buffer. Captured proteins were eluted and cross-links were reversed in SDS sample buffer by incubating for 25 min at 95°C . Proteins were resolved on SDS-PAGE and detected by immunoblotting. Rabbit α -Rad51 (1:1000), mouse α -PCNA (1:1000), mouse α -FLAG (1:1000), and rabbit α -histone H3 (1:3000) in block buffer were respectively applied to probe proteins at 4°C overnight. After washes with TBS-T buffer three times, the membranes were incubated with secondary antibodies (α -Rabbit 680RD and anti-mouse 800CW, 1:10000) for 2 hr, washed with TBS for 3 times, and obtained images on Odyssey Imaging System (Li-Cor Biosciences).

TREX2^{H188A} pulldown with UBC13

In vitro GST pull-down assays was performed as described (Hu et al., 2013). GST-MMS2, GST-UBC13, and GST-TREX2^{H188A} fusion proteins (5 μg) were bound to glutathione-Sepharose 4B (GE Healthcare) and incubated with [³⁵S]-methionine-labeled TREX2 (4 μL) for 1.5 hr at 23°C as previously described (Kim et al., 2010). The beads were washed with NETN buffer (50 mM Tris, 250 mM NaCl, 5 mM EDTA, pH 7.5, and 0.1% NP40) and subjected to SDS-PAGE and phosphorimager analysis.

PCNA ubiquitination

Isolated chromatin-bound fraction as described (Krijger et al., 2011; Motegi et al., 2008) with modifications. Briefly, resuspend $\sim 1.5 \times 10^7$ cells in buffer A [10 mM HEPES (pH 7.9), 1.5 mM MgCl_2 , 10 mM KCl, 0.34 M sucrose, 10% glycerol, 0.1% Triton X-100 and protease inhibitor cocktail (Roche)], incubate and rotate 5 min at 4°C then centrifuge (7000 rpm, 2 min, 4°C). Remove soluble fraction. Resuspended pellet in buffer then centrifuge (7000 rpm, 3 min, 4°C). Extract chromatin-bound fraction, resuspend pellet in buffer B [20 mM Tris-Cl (pH 8.1), 2 mM EDTA (pH 8.0), 500 mM NaCl, 0.1% SDS, 1% Triton X-100 and protease inhibitor cocktail (Roche)], sonicate, treat with micrococcal nuclease (10 min, 37°C) and centrifuge (13000 rpm, 15 min, 4°C). Immunoprecipitated supernatant containing released chromatin-bound protein. Pre-incubate with protein G Sepharose beads (GE healthcare) (1–2 hr, 4°C) to pre-cleaned protein and incubated with 1 μg of anti-PCNA antibody (PC10, Santa Cruz Biotechnology) overnight at 4°C . Precipitate anti-PCNA immune complexes with 30 μL protein G Sepharose beads for 3 hours at 4°C . Separate protein on 10% SDS-PAGE gel and transfer onto PVDF membrane. Use monoclonal antibodies for western blot: anti-Ub (P4D1, 1:1000–2000) or anti-PCNA (PC10, 1: 2000–2500). Used mouse True[®]Blot ULTRA (Anti-mouse Ig HRP, 1:1000–2500) to minimize IgG signal. Quantify band intensities with ImageJ software (<http://imagej.nih.gov/ij/>).

QUANTIFICATION AND STATISTICAL ANALYSIS

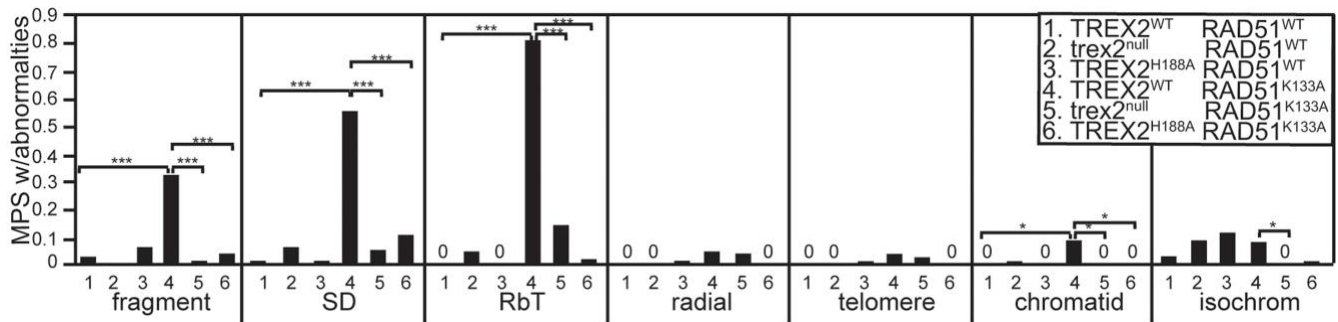
The statistical analysis was performed using Prism8 software (GraphPad). For two-color FISH assay, Chi-square with Yates' correction and Fisher's exact test were used. For miniHPRT LOF, unpaired t test and one-way ANOVA with Tukey's or Sidák's multiple comparisons test. For colony forming assay, two-way ANOVA with Dunnett's multiple comparisons test were used. For DNA fiber assay, Chi-square with Yates' correction and Fisher's exact test were used in replication fork stalling. Kruskal-Wallis test with Dunn's multiple comparisons test were used for nascent DNA degradation.

Cell Reports, Volume 33

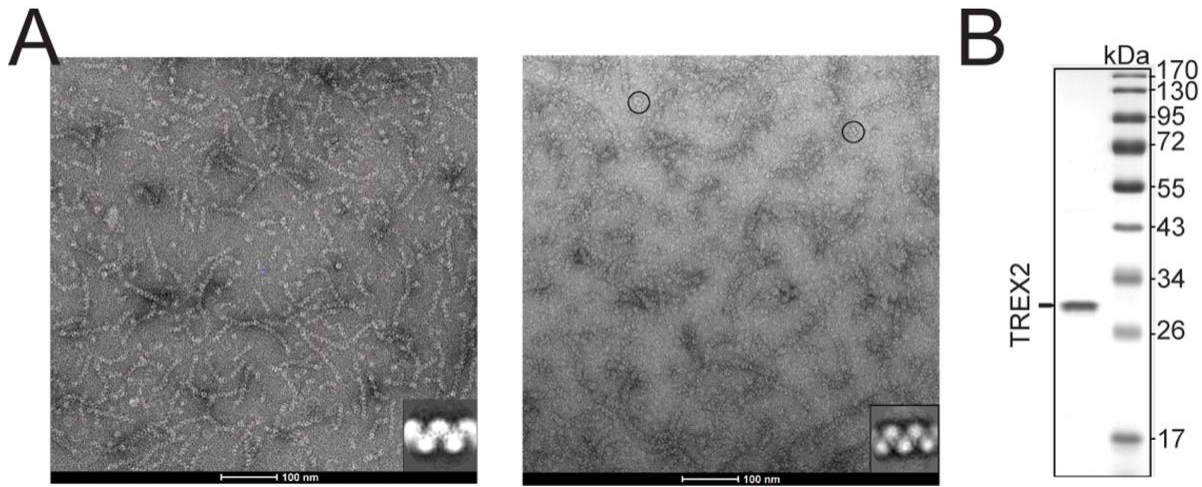
Supplemental Information

TREX2 Exonuclease Causes Spontaneous Mutations and Stress-Induced Replication Fork Defects in Cells Expressing RAD51^{K133A}

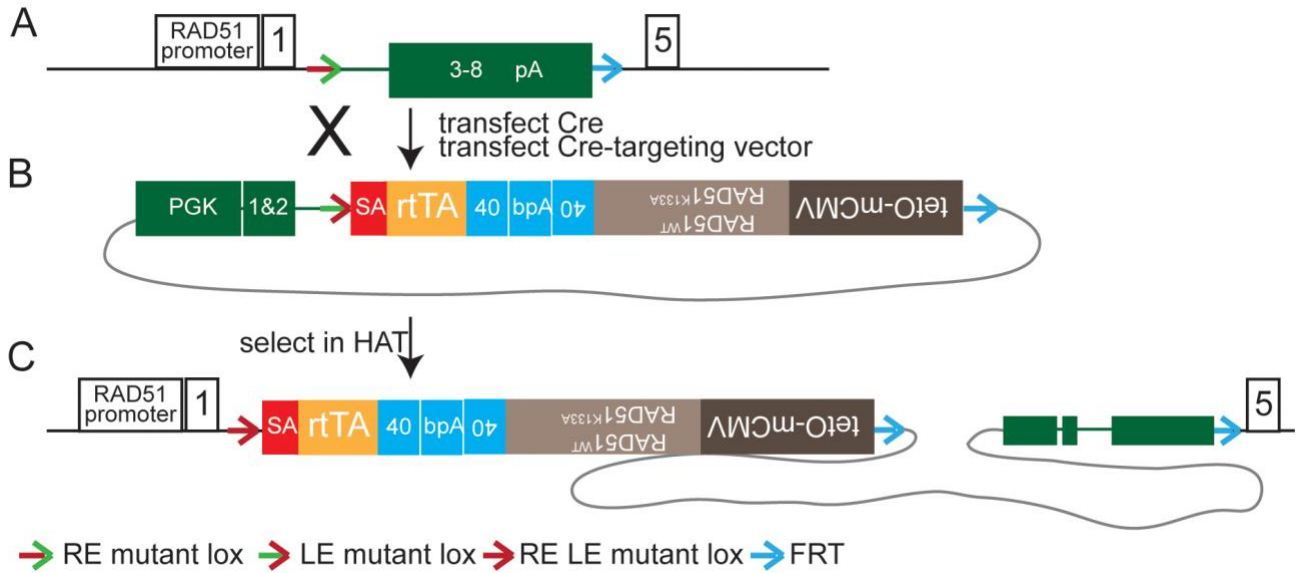
Jun Ho Ko, Mi Young Son, Qing Zhou, Lucia Molnarova, Lambert Song, Jarmila Mlcouskova, Atis Jekabsons, Cristina Montagna, Lumir Krejci, and Paul Hasty



Supplemental Fig. 1. Quantification of effect of TREX2-deletion or TREX2^{H188A} expression on specific chromosomal aberrations in RAD51^{K133A} cells shown in figure 2A. Statistics: Chi-square with Yates' correction and a Fisher's exact test were performed using Prism8 software (GraphPad). At least 60 MPSs were analyzed and counted for each genotype. Statistics are represented by * p<0.05, ** p<0.005, *** p<0.0005. Related to figure 2A.



Supplemental Fig. 2. Demonstration of RAD51^{K133A} filaments and TREX2^{WT} protein purification. (A) Electron micrographs showing RAD51^{WT} (left) and RAD51^{K133A} (right) filaments and rings formed on short DNA substrate with 35 bases overhang. RAD51^{K133A} protein rings are highlighted in black circles. Inset shows a two-dimensional class average of 727 filament segments (segment size 243 angstroms). (B) Coomassie Blue staining of purified TREX2 used in the study. Related to STAR Methods.



Supplemental Fig. 3. Schematics of inducible RAD51^{WT} and RAD51^{K133A}. (A) *Rad51* exons 3-4 are targeted with a floxed *miniHPRT* and the 5' half of *miniHPRT* was removed with Cre recombinase (taken from figure 1B1). (B) Knockin of Cre-mediated targeting vector that places rtTA adjacent to the *Rad51* promoter and with an inducible tetO-mCMV expression cassette in reverse orientation that expresses either RAD51^{WT} and RAD51^{K133A}. Select in HAT and screen for knockin by PCR. (C) The final product. Related to STAR Methods.